

5. SYNTHESIS OF SERIES I

5. Synthesis - Series I-Indole Thiazolidinedione hybrid analogues

5.1. Rationale

PL inhibition-based bioactivity guided fractionation of methanol extract of *A. scholaris* stem bark resulted in the identification of echitamine as a potential natural product lead. Further, this fact was supported by the molecular modelling studies and a positive correlation between the echitamine content and respective PL inhibition. Based on these results, an *in-silico* analysis of echitamine and orlistat was performed using human PL (PDB ID: 1LPB) and the results are represented in **Fig. 5.1**.

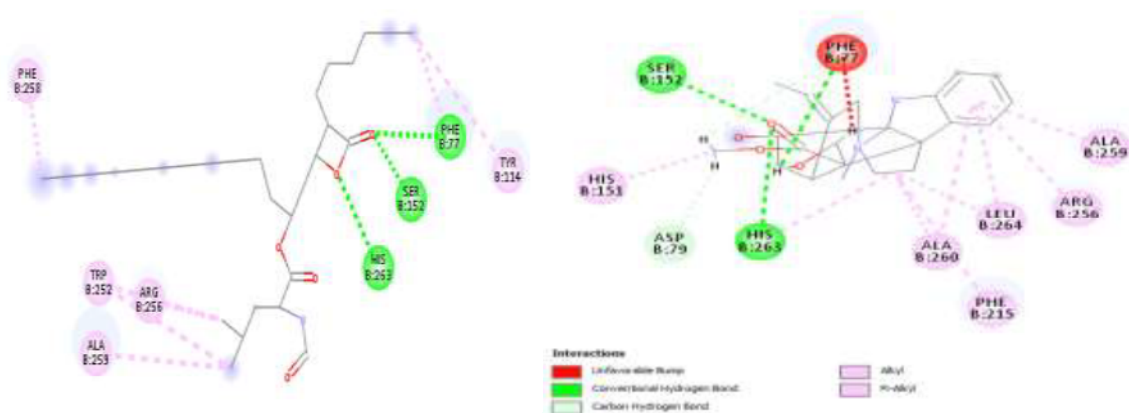


Fig. 5.1. 2-D interaction diagram of Orlistat and Echitamine with the active site of PL (1LPB0)

Orlistat and Echitamine exhibited MolDock Scores of -107.75 Kcal/mol & -43.44 Kcal/mol, respectively. A structural comparison of these molecules with respect to their PL inhibition potential highlighted that the echitamine lacked a reactive carbonyl group. Potential chemical functionalities having an ability to interact with Ser-152 is essential requirement for the PL inhibition. Orlistat possessed a highly reactive β -lactone, while echitamine contained a simple methyl ester. This might be the putative reason for a lower PL inhibitory potential of the echitamine. Additionally, due to the structural rigidity of echitamine, an unfavourable interaction was observed with the lid domain amino acid (Phe 77) of PL. Thus, potent PL inhibitors can be developed by the various structural modifications such as the reducing the structural rigidity, incorporation of the reactive functionalities and various essential pharmacophoric features, that is required for PL inhibition.

Previously various analogues containing indole scaffold have been reported (**Fig. 5.2.**) to be effective against the metabolic conditions [1–4]. Our group explored the significant

Chapter V

role of structural modification of carbazole (inspired from conophylline) to indole scaffold for generation of potent PL inhibitors [4,5]. This study revealed the effect of reduction of the structural rigidity *viz* replacing a carbazole (DK-5; $IC_{50} = 6.31 \mu M$) to an indole scaffold (AP-21), wherein the latter analogue exhibited a higher PL inhibitory potential ($IC_{50} = 4.92 \mu M$). Thus, we presumed that the structural rigidity of echitamine can also be reduced by selecting indole scaffold as a pharmacophore for the hybrid drug discovery.

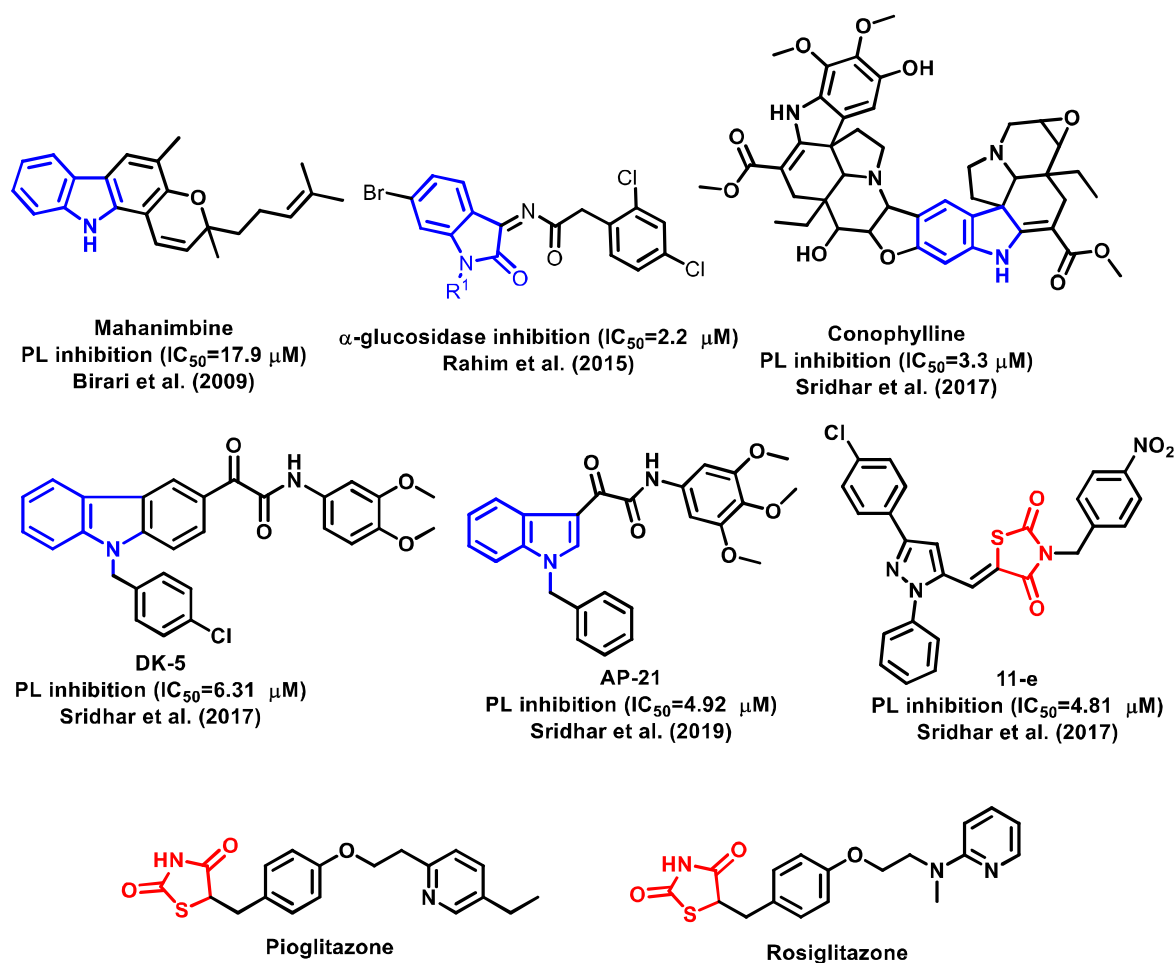


Fig. 5.2. Structures of some indole and TZD containing analogues reported for metabolic disease (insight represent the pharmacophoric design of the target analogues).

Literature review revealed that numerous chemical functionalities have been explored as a chemical warhead for potential PL inhibition. These include fluorinated ketones, α -keto esters, α -ketoamides and 1,2-diketones etc., that offers a reactive carbonyl group for interacting with Ser 152 [6,7]. Apart from these, various nitrogen containing heterocycles (oxadiazoles, 1,3-pyrazoles, 2,4-thiazolidinediones) have also been reported for their

potential PL inhibition [8,9]. Amongst these heterocycles, thiazolidinediones (TZD) or glitazones are the privileged fragments in the discovery of novel drug candidates (**Fig. 5.2.**) for the treatment of metabolic disorders [10,11]. Further, TZD also offers an advantage of a reactive nitrogen in the form of imide linkage. These chemical benefits can be fruitfully explored for the echitamine inspired analogues, wherein the imide linkage can offer a higher stability over the simple methyl ester of echitamine. Further, it is expected that the imide linkage can offer a reactive carbonyl group for interacting with Ser 152. Previously, our group has identified the role of TZD in the PL inhibition [12]. Amongst the screened analogues diaryl substituted pyrazolyl TZD exerted a potential PL inhibitory activity ($IC_{50} = 4.81 \mu\text{M}$)

Hence, based on these observations, we hypothesized the indole-TZD hybrid analogues to possess potential PL inhibitory activity. The designing strategy mainly relied on molecular hybridisation approach, wherein the structural rigidity of echitamine was reduced by constricting the ring size as well as incorporation of the active pharmacophoric functionality such as TZD (**Fig. 5.3**). Thus, the present chapter briefs about the syntheses of a series of indole-TZD hybrid analogues followed by their *in-vitro* PL inhibition and molecular modelling studies.

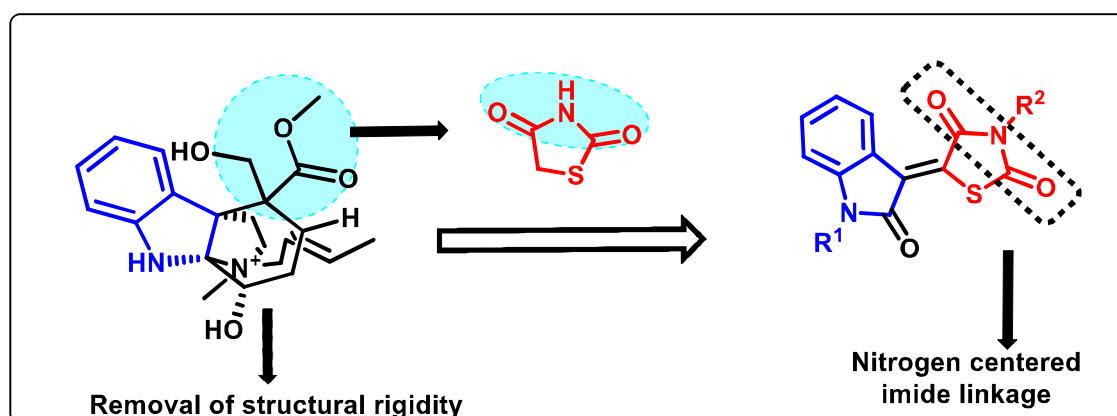


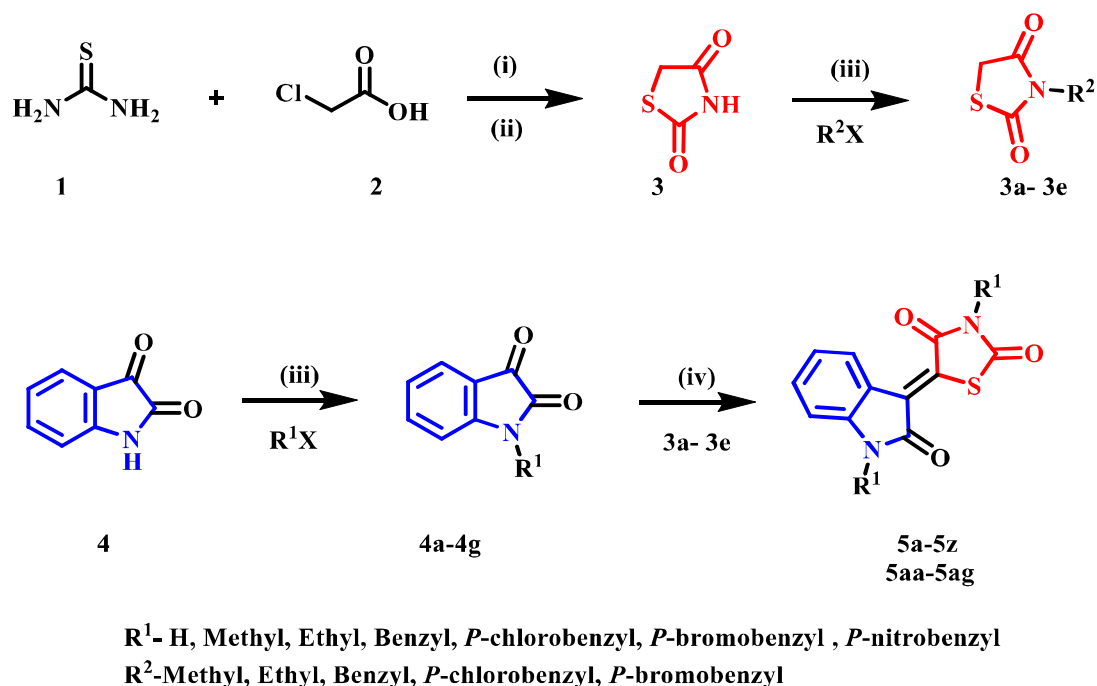
Fig. 5.3. Rationale for the designing of the hybrid analogues

5.2. Synthesis and Characterisation

The route for the synthesis of the analogues (**5a – 5ag**) is depicted in **Scheme 5.1**. TZD (**3**) was prepared according to the literature [12]. Condensation of thiourea (**1**) with chloroacetic acid (**2**) at 0-5 °C resulted in the formation of 2-iminothiazolidine-4-dione (white ppt), that upon further refluxing with conc. HCl for 10-12 h resulted in the formation of 2,4-TZD (**3**) as white fine crystals. *N* (**3**)- alkylation of TZDs was carried out by treating TZD with NaH followed by the addition of alkyl/aryl halides. After the

Chapter V

specified time, the reaction mixture was poured into ice-cold water resulting in the formation of *N*-substituted 2,4-TZD (**3a-3e**) [13,14]. Treatment of isatin (**4**) with various halides in the presence of NaH in DMF resulted in the formation of *N*-substituted isatin derivatives (**4a-4g**). Treatment of *N*-substituted 2,4-TZD (**3a-3e**) with isatin and their *N*-substituted derivatives (**4**, **4a-4g**) in methanol and few drops of 40% KOH resulted in the formation of corresponding indole-TZD hybrid analogues (**5a to 5ag**) [15,16].



Scheme 5.1. Synthesis of series I analogues (**5a - 5ag**). Reagents and conditions (i) 0-5°C, 30 min; (ii) HCl, H₂O, 110-120 °C, 10-12 h; (iii) NaH, DMF, 12 h; (iv) KOH, MeOH, 2-3 h, RT

General procedure for the synthesis of thiazolidine-2,4-dione (3)

A solution of thiourea (4.56 g in 6 mL, 59.91 mmol) and chloroacetic acid (5.6 g in 6 mL, 59.91 mmol) in water was stirred for 30 min to obtain a white precipitate accompanied by considerable cooling. To the resulting precipitate, 5 mL of conc. HCl was added and the reaction mixture was refluxed (100–110 °C for 10-12 h). White needle-shaped crystals of TZD separated during cooling. Traces of the acids were removed by washing with water and product was recrystallized from ethanol, if required [14].

General procedure for the synthesis of N-substituted thiazolidine-2,4-dione derivatives (3a-3e)

Condensation of thiazolidine-2,4-dione (1 eq.) with various alkyl/aryl halides (1.5 eq.) was performed in the presence of NaH (1.5 eq.) in anhydrous DMF. After the specified time of

Chapter V

stirring, the solution was poured into the ice-cold water and the obtained precipitate was filtered and recrystallised from the appropriate solvents [17].

General procedure for the synthesis of N-substituted isatin derivatives (4a-4g)

N-substituted isatin derivatives were prepared by N-alkylation of isatin as the starting material in anhydrous DMF and NaH.

General procedure for the synthesis of indole- TZD analogues (5a to 5ag)

To a mixture of 1.0 eq. of indole derivatives and 1.5 eq. of 1,3-thiazolidine-2,4-dione in methanol (20 mL), a catalytic amount of 40% KOH was added, and the reaction mixture was stirred at room temperature for 2-3 h. The obtained crude precipitate was filtered, recrystallized from chloroform-methanol mixture or purified by column chromatography by using hexane: ethyl acetate [15,18]

Characterisation

The synthesized analogues (**5a** to **5ag**) were obtained in good yield with a vermilion red colour. Further, they were characterized by ATR, ^1H , ^{13}C NMR spectroscopy and mass spectrometry HRMS [ESI mode]. The obtained data were in good agreement with their structural identity. The IR spectrum of the analogues (**5a** to **5ag**) showed a strong absorption bands at 1723-1744 cm^{-1} and 1643-1680 cm^{-1} that were assigned to the carbonyl groups. The disappearance of methylene protons (3.95 δ ppm) of TZD further confirmed its reaction with isatin. The $-\text{CH}_2$ proton attached to the TZD resonated in the range of 3.71 to 5.11 δ ppm, while the terminal $-\text{CH}_3$ proton resonated at a range of 3.14 to 3.34 δ ppm. $-\text{CH}_2$ proton attached to the indoline-2-one resonated in the range of 3.33 to 5.12 δ ppm. All other protons were observed in expected regions. The appearance of three $\text{C}=\text{O}$ peaks in ^{13}C NMR (165 to 170 δ ppm) further confirmed the reaction progress of TZD and indole scaffolds. All the analogues showed prominent signals in the range of 12-49 δ ppm due to the presence of various alkyl groups. A “Z” isomeric configuration was obtained between arylidene double bond amongst the isatin and TZD. This fact can be supported by the downfield shift of H_4 of isatin scaffold (≈ 9 δ ppm), that might be due to the hydrogen bond formation with the carbonyl functionality of TZD. Apart from this, the configuration can be ascribed due to the favourable electrostatic interactions between the C_2 carbonyl oxygen atom of isatin and partially positively charged “S” of TZD heterocycles [13,16,19,20]. Detailed information on characterisation of all the analogues are given below.

***(Z)*-3-Methyl-5-(2-oxoindolin-3-ylidene)thiazolidine-2,4-dione (5a)**

Yield: 55%; Vermilion red solid; m.p: 278-280 °C; ¹H NMR (400 MHz, DMSO-*d*₆) δ 11.26 (s, 1H, -NH), 8.83 (d, *J* = 7.9 Hz, 1H, -H₄ of Indolin-2-one), 7.42 (t, *J* = 7.7 Hz, 1H, -H₅ of Indolin-2-one), 7.11 (t, *J* = 7.8 Hz, 1H, -H₆ of Indolin-2-one), 6.97 (d, *J* = 7.8 Hz, 1H, -H₇ of Indolin-2-one), 3.14 (s, 3H, -CH₃); ¹³C NMR (100 MHz, DMSO-*d*₆) δ 170.52, 168.83, 166.18, 144.33, 133.17, 130.63, 128.33, 127.22, 122.57, 120.33, 111.01, 27.78; IR (ATR) ν 3139, 3071, 2884, 2353, 1680, 1616, 1427, 1351, 1293, 1233, 1081, 1006, 753, 673 cm⁻¹; HRMS (ESI⁺) calculated for C₁₂H₈N₂O₃S [M+H]⁺, 261.0256; found 261.0251.

***(Z)*-3-Methyl-5-(1-methyl-2-oxoindolin-3-ylidene)thiazolidine-2,4-dione (5b)**

Yield: 82%; Vermilion red solid; m.p: 254-258 °C; ¹H NMR (400 MHz, CDCl₃) δ 8.98 (d, *J* = 7.7 Hz, 1H, -H₄ of Indolin-2-one), 7.46 (t, *J* = 7.8 Hz, 1H, -H₅ of Indolin-2-one), 7.17 (t, *J* = 7.7 Hz, 1H, -H₆ of Indolin-2-one), 6.91 (d, *J* = 7.8 Hz, 1H, -H₇ of Indolin-2-one), 3.33 (s, 3H, -CH₃), 3.32 (s, 3H, -CH₃); ¹³C NMR (100 MHz, CDCl₃) δ 170.20, 167.47, 165.82, 145.00, 132.56, 130.70, 128.67, 127.39, 123.20, 119.86, 108.39, 27.46, 26.45; IR (ATR) ν 2353, 1731, 1664, 1600, 1477, 1427, 1363, 1274, 1140, 1075, 1007, 870, 750, 667 cm⁻¹; HRMS (ESI⁺) calculated for C₁₃H₁₀N₂O₃S [M+H]⁺, 275.0412; found 275.0475.

***(Z)*-5-(1-Ethyl-2-oxoindolin-3-ylidene)-3-methylthiazolidine-2,4-dione (5c)**

Yield: 75%; Vermilion red solid; m.p: 142-144 °C; ¹H NMR (400 MHz, CDCl₃) δ 8.96 (dd, *J* = 7.9, 1.3 Hz, 1H, -H₄ of Indolin-2-one), 7.43 (td, *J* = 7.7, 1.3 Hz, 1H, -H₅ of Indolin-2-one), 7.14 (td, *J* = 7.7, 1.1 Hz, 1H, -H₆ of Indolin-2-one), 6.91 (d, *J* = 7.8 Hz, 1H, -H₇ of Indolin-2-one), 3.86 (q, *J* = 7.2 Hz, 2H, -CH₂ attached to Indolin-2-one), 3.29 (s, 3H, -CH₃ attached to TZD), 1.33 (t, *J* = 7.2 Hz, 3H, -CH₃ attached Indolin-2-one); ¹³C NMR (100 MHz, CDCl₃) δ 170.24, 167.05, 165.79, 144.12, 132.49, 130.51, 128.84, 127.46, 122.94, 120.02, 108.49, 35.14, 27.43, 12.76; IR (ATR) ν 2355, 1735, 1664, 1600, 1462, 1423, 1357, 1276, 1228, 1142, 1071, 1003, 942, 749, 655 cm⁻¹; HRMS (ESI⁺) calculated for C₁₄H₁₂N₂O₃S [M+H]⁺, 289.0569; found 289.0631

***(Z)*-5-(1-Benzyl-2-oxoindolin-3-ylidene)-3-methylthiazolidine-2,4-dione (5d)**

Yield: 70%; Vermilion red solid; m.p: 164-165 °C; ¹H NMR (400 MHz, CDCl₃) δ 8.99 (dd, *J* = 7.9, 1.2 Hz, 1H, -H₄ of Indolin-2-one), 7.38 – 7.29 (m, 6H), 7.13 (td, *J* = 7.8, 1.1 Hz, 1H, -H₆ of Indolin-2-one), 6.83 – 6.79 (m, 1H), 5.01 (s, 2H, -CH₂ attached to Indolin-2-one), 3.31 (s, 3H, -CH₃ attached to TZD); ¹³C NMR (100 MHz, CDCl₃) δ 170.09,

167.59, 165.77, 144.17, 135.09, 132.50, 131.05, 128.93, 128.75, 127.95, 127.33, 127.22, 123.21, 120.02, 109.39, 44.15, 27.49 IR (ATR) ν 2915, 2850, 2355, 1733, 1669, 1603, 1464, 1424, 1359, 1278, 1189, 1081, 1011, 748, 677 cm^{-1} ; HRMS (ESI⁺) calculated for C₁₉H₁₄N₂O₃S [M+H]⁺, 351.0725; found 351.0770.

(Z)-5-(1-(4-Chlorobenzyl)-2-oxoindolin-3-ylidene)-3-methylthiazolidine-2,4-dione (5e)

Yield: 65%; Vermilion red solid; m.p: 218-220 °C; ¹H NMR (400 MHz, CDCl₃) δ 9.00 (dd, $J = 7.9, 1.2$ Hz, 1H, -H₄ of Indolin-2-one), 7.40 – 7.30 (m, 3H), 7.28 – 7.24 (m, 2H), 7.15 (td, $J = 7.8, 1.1$ Hz, 1H, -H₆ of Indolin-2-one), 6.82 – 6.74 (m, 1H), 4.98 (s, 2H, -CH₂ attached to Indolin-2-one), 3.32 (s, 3H, -CH₃ attached to TZD); ¹³C NMR (100 MHz, CDCl₃) δ 169.94, 167.60, 165.74, 143.82, 133.89, 133.60, 132.50, 131.34, 129.13, 128.87, 128.72, 127.02, 123.40, 120.05, 109.18, 43.52, 27.52; IR (ATR) ν 2926, 2855, 2356, 1738, 1674, 1607, 1428, 1359, 1285, 1184, 1088, 1014, 872.5, 795, 752 cm^{-1} ; HRMS (ESI⁺) calculated for C₁₉H₁₃ClN₂O₃S [M+H]⁺, 385.0335; found 385.0382.

(Z)-5-(1-(4-Bromobenzyl)-2-oxoindolin-3-ylidene)-3-methylthiazolidine-2,4-dione (5f)

Yield: 60%; Vermilion red solid; m.p: 188-200 °C; ¹H NMR (400 MHz, CDCl₃) δ 9.01 (dd, $J = 7.9, 1.2$ Hz, 1H, -H₄ of Indolin-2-one), 7.51 – 7.45 (m, 2H), 7.36 (td, $J = 7.8, 1.3$ Hz, 1H, -H₆ of Indolin-2-one), 7.22 – 7.12 (m, 3H), 6.78 (dt, $J = 7.8, 0.8$ Hz, 1H, -H₇ of Indolin-2-one), 4.97 (s, 2H, -CH₂ attached to Indolin-2-one), 3.33 (s, 3H, -CH₃ attached to TZD); ¹³C NMR (100 MHz, CDCl₃) δ 170.11, 167.51, 166.01, 144.01, 138.37, 135.79, 133.00, 132.12, 131.96, 130.13, 130.02, 128.28, 125.97, 123.38, 121.24, 119.86, 110.29, 43.02, 27.89; IR (ATR) ν 2356, 1733, 1674, 1608, 1467, 1427, 1357, 1286, 1182, 1082, 1010, 943, 752, 672 cm^{-1} ; HRMS (ESI⁺) calculated for C₁₉H₁₃BrN₂O₃S [M+H]⁺, 428.9830; found 428.9862

(Z)-3-Methyl-5-(1-(4-nitrobenzyl)-2-oxoindolin-3-ylidene)thiazolidine-2,4-dione (5g)

Yield: 62%; Vermilion red solid; m.p: 242-245 °C; ¹H NMR (400 MHz, CDCl₃) δ 9.05 (dd, $J = 7.9, 1.1$ Hz, 1H, -H₄ of Indolin-2-one), 8.29 – 8.18 (m, 2H), 7.53 – 7.46 (m, 2H), 7.38 (td, $J = 7.8, 1.3$ Hz, 1H, -H₆ of Indolin-2-one), 7.19 (td, $J = 7.8, 1.1$ Hz, 1H), 6.75 (d, $J = 7.8$ Hz, 1H, -H₇ of Indolin-2-one), 5.12 (s, 2H, -CH₂ attached to Indolin-2-one), 3.34 (s, 3H, -CH₃ attached to TZD); ¹³C NMR (100 MHz, CDCl₃) δ 169.70, 167.67, 165.67, 147.74, 143.36, 142.41, 132.57, 131.92, 129.08, 128.05, 126.64, 124.24, 123.74, 120.11, 108.88, 43.52, 27.59; IR (ATR) ν 2916, 2849, 2356, 1732, 1670, 1603, 1518, 1426, 1346,

1280, 1184, 1087, 1014, 868, 747, 674 cm^{-1} ; HRMS (ESI⁺) calculated for C₁₉H₁₃N₃O₅S [M+H]⁺, 396.0576; found 396.0627

(Z)-3-Ethyl-5-(2-oxoindolin-3-ylidene)thiazolidine-2,4-dione (5h)

Yield: 52%; Vermilion red solid; m.p: 234-236 °C; ¹H NMR (400 MHz, DMSO-*d*₆) δ 11.23 (s, 1H, -NH), 8.80 (dd, *J* = 8.0, 1.2 Hz, 1H, -H₄ of Indolin-2-one), 7.40 (td, *J* = 7.7, 1.3 Hz, 1H, -H₅ of Indolin-2-one), 7.08 (td, *J* = 7.7, 1.1 Hz, 1H, -H₆ of Indolin-2-one), 6.95 (d, *J* = 7.8 Hz, 1H, -H₇ of Indolin-2-one), 3.71 (q, *J* = 7.2 Hz, 2H, -CH₂ attached to TZD), 1.19 (t, *J* = 7.2 Hz, 3H, -CH₃); ¹³C NMR (100 MHz, DMSO-*d*₆) δ 170.30, 168.75, 165.81, 144.34, 133.15, 130.45, 128.37, 127.33, 122.51, 120.30, 110.96, 36.63, 13.13; IR (ATR) ν 3780, 3707, 2915, 2847, 2356, 1657, 1442, 1376, 1228, 1078, 1032, 794, 745 cm^{-1} ; HRMS (ESI⁺) calculated for C₁₃H₁₀N₂O₃S [M+H]⁺, 275.0412; found 275.0457

(Z)-3-Ethyl-5-(1-methyl-2-oxoindolin-3-ylidene)thiazolidine-2,4-dione (5i)

Yield: 68%; Vermilion red solid; m.p: 248-250 °C; ¹H NMR (400 MHz, CDCl₃) δ 8.99 (d, *J* = 7.9 Hz, 1H, -H₄ of Indolin-2-one), 7.46 (t, *J* = 7.7 Hz, 1H, -H₅ of Indolin-2-one), 7.17 (t, *J* = 7.8 Hz, 1H, -H₆ of Indolin-2-one), 6.91 (d, *J* = 7.9 Hz, 1H, -H₇ of Indolin-2-one), 3.90 (q, *J* = 7.2 Hz, 2H, -CH₂ attached to TZD), 3.33 (s, 3H, -CH₃ attached to Indolin-2-one), 1.33 (t, *J* = 7.2 Hz, 3H, -CH₃); ¹³C NMR (100 MHz, CDCl₃) δ 169.96, 167.50, 165.60, 144.97, 132.46, 131.01, 128.67, 127.24, 123.15, 119.91, 108.34, 36.68, 26.42, 13.08; IR (ATR) ν 3780, 3707, 2356, 1662, 1599, 1441, 1379, 1340, 1137, 1071, 958, 793 cm^{-1} ; HRMS (ESI⁺) calculated for C₁₄H₁₂N₂O₃S [M+H]⁺, 289.0569; found 289.0611

(Z)-3-Ethyl-5-(1-ethyl-2-oxoindolin-3-ylidene)thiazolidine-2,4-dione (5j)

Yield: 63%; Vermilion red solid; m.p: 172-175 °C; ¹H NMR (400 MHz, CDCl₃) δ 8.98 (d, *J* = 7.9 Hz, 1H, -H₄ of Indolin-2-one), 7.43 (t, *J* = 7.7 Hz, 1H, -H₅ of Indolin-2-one), 7.13 (d, *J* = 7.8 Hz, 1H, -H₆ of Indolin-2-one), 6.91 (d, *J* = 7.9 Hz, 1H, -H₇ of Indolin-2-one), 3.87 (p, *J* = 7.1 Hz, 4H, -CH₂), 1.32 (td, *J* = 7.3, 2.6 Hz, 6H, -CH₃); ¹³C NMR (100 MHz, CDCl₃) δ 169.98, 167.11, 165.59, 144.10, 132.39, 130.84, 128.86, 127.36, 122.91, 120.10, 108.43, 36.64, 35.11, 13.07, 12.72; IR (ATR) ν 3779, 3704, 2356, 1730, 1658, 1341, 1227, 1072, 793, 669 cm^{-1} ; HRMS (ESI⁺) calculated for C₁₅H₁₄N₂O₃S [M+H]⁺, 303.0725; found 303.0769

(Z)-5-(1-Benzyl-2-oxoindolin-3-ylidene)-3-ethylthiazolidine-2,4-dione (5k)

Yield: 62%; Vermilion red solid; m.p: 160-164 °C; ¹H NMR (400 MHz, CDCl₃) δ 9.01 (dd, *J* = 7.9, 1.2 Hz, 1H, -H₄ of Indolin-2-one), 7.40 – 7.29 (m, 6H), 7.14 (td, *J* = 7.8, 1.1 Hz, 1H, -H₆ of Indolin-2-one), 6.86 – 6.78 (m, 1H), 5.02 (s, 2H, -CH₂ attached to Indolin-2-one), 3.91 (q, *J* = 7.2 Hz, 2H, -CH₂ attached to TZD), 1.33 (t, *J* = 7.2 Hz, 3H, -CH₃); ¹³C NMR (100 MHz, CDCl₃) δ 169.89, 167.65, 165.60, 144.13, 135.11, 132.43, 131.37, 128.92, 128.77, 127.93, 127.31, 127.13, 123.20, 120.07, 109.36, 44.13, 36.72, 13.11; IR (ATR) ν 2916, 1728, 1665, 1603, 1457, 1347, 1220, 1178, 1083, 861, 749, 695 cm⁻¹; HRMS (ESI⁺) calculated for C₂₀H₁₆N₂O₃S [M+H]⁺, 365.0882; found 365.0932

(Z)-5-(1-(4-Bromobenzyl)-2-oxoindolin-3-ylidene)-3-ethylthiazolidine-2,4-dione 5l)

Yield: 64%; Vermilion red solid; m.p: 202-203 °C; ¹H NMR (400 MHz, CDCl₃) δ 9.01 (dd, *J* = 8.0, 1.2 Hz, 1H, -H₄ of Indolin-2-one), 7.51 – 7.43 (m, 2H), 7.35 (td, *J* = 7.7, 1.2 Hz, 1H, -H₅ of Indolin-2-one), 7.24 – 7.11 (m, 3H), 6.81 – 6.74 (m, 1H), 4.96 (s, 2H, -CH₂ attached to Indolin-2-one), 3.90 (q, *J* = 7.2 Hz, 2H, -CH₂ attached to TZD), 1.33 (t, *J* = 7.2 Hz, 3H, -CH₃); ¹³C NMR (100 MHz, CDCl₃) δ 169.72, 167.62, 165.52, 143.75, 134.16, 132.43, 132.08, 131.67, 129.02, 128.88, 126.87, 123.38, 121.94, 120.07, 109.15, 43.55, 36.76, 13.10; IR (ATR) ν 2915, 2849, 2352, 1667, 1602, 1455, 1358, 1220, 1183, 1080, 1007, 792, 745 cm⁻¹; HRMS (ESI⁺) calculated for C₂₀H₁₅BrN₂O₃S [M+H]⁺, 442.9987; found 443.0019

(Z)-5-(1-(4-Chlorobenzyl)-2-oxoindolin-3-ylidene)-3-ethylthiazolidine-2,4-dione (5m)

Yield: 58%; Vermilion red solid; m.p: 208-210 °C; ¹H NMR (400 MHz, CDCl₃) δ 9.00 (ddd, *J* = 7.9, 1.3, 0.6 Hz, 1H, -H₄ of Indolin-2-one), 7.38 – 7.29 (m, 3H), 7.26 (d, *J* = 2.2 Hz, 1H, -H₆ of Indolin-2-one), 7.24 (q, *J* = 1.9 Hz, 1H), 7.14 (td, *J* = 7.7, 1.1 Hz, 1H), 6.77 (dt, *J* = 7.8, 0.9 Hz, 1H), 4.97 (s, 2H, -CH₂ attached to Indolin-2-one), 3.89 (q, *J* = 7.2 Hz, 2H, -CH₂ attached to TZD), 1.33 (t, *J* = 7.2 Hz, 3H, -CH₃); ¹³C NMR (100 MHz, CDCl₃) δ 169.71, 167.61, 165.52, 143.77, 133.87, 133.64, 132.42, 131.65, 129.12, 128.87, 128.70, 126.87, 123.36, 120.07, 109.15, 43.49, 36.75, 13.10; IR (ATR) ν 3726, 2356, 1734, 1672, 1605, 1462, 1365, 1224, 1186, 1089, 863, 794, 670 cm⁻¹; HRMS (ESI⁺) calculated for ; HRMS (ESI⁺) calculated for C₂₀H₁₅ClN₂O₃S [M+H]⁺, 399.0492; found 399.0527.

(Z)-3-Ethyl-5-(1-(4-nitrobenzyl)-2-oxoindolin-3-ylidene)thiazolidine-2,4-dione (5n)

Yield: 58%; Vermilion red solid; m.p: 160-164 °C; ¹H NMR (400 MHz, CDCl₃) δ 9.01 (dd, *J* = 7.9, 1.2 Hz, 1H, -H₄ of Indolin-2-one), 7.40 – 7.29 (m, 6H), 7.14 (td, *J* = 7.8, 1.1 Hz, 1H, -H₆ of Indolin-2-one), 6.86 – 6.78 (m, 1H), 5.02 (s, 2H, -CH₂ attached to Indolin-2-one), 3.91 (q, *J* = 7.2 Hz, 2H, -CH₂ attached to TZD), 1.33 (t, *J* = 7.2 Hz, 3H, -CH₃); ¹³C NMR (100 MHz, CDCl₃) δ 169.89, 167.65, 165.60, 144.13, 135.11, 132.43, 131.37, 128.92, 128.77, 127.93, 127.31, 127.13, 123.20, 120.07, 109.36, 44.13, 36.72, 13.11; IR (ATR) ν 2916, 1728, 1665, 1603, 1457, 1347, 1220, 1178, 1083, 861, 749, 695 cm⁻¹; HRMS (ESI⁺) calculated for C₂₀H₁₅N₃O₅S [M+H]⁺, 410.4160; found 410.0770

(Z)-3-Benzyl-5-(2-oxoindolin-3-ylidene)thiazolidine-2,4-dione (5o)

Yield: 52%; Vermilion red solid; m.p: 298-300 °C; ¹H NMR (400 MHz, DMSO-*d*₆) δ 11.27 (s, 1H, -NH), 8.81 (d, *J* = 7.9 Hz, 1H, -H₄ of Indolin-2-one), 7.45 – 7.29 (m, 6H), 7.10 (t, *J* = 7.7 Hz, 1H, -H₆ of Indolin-2-one), 6.97 (d, *J* = 7.8 Hz, 1H, -H₇ of Indolin-2-one), 4.89 (s, 2H); ¹³C NMR (100 MHz, DMSO-*d*₆) δ 175.30, 173.52, 170.67, 149.25, 143.68, 140.59, 138.81, 138.12, 133.87, 133.21, 132.99, 132.94, 127.35, 125.06, 115.81, 49.49; IR (ATR) ν 3852, 3746, 3150, 2918, 2852, 1744, 1665, 1540, 1453, 1379, 1331, 1228, 1146, 1071, 1028, 955, 889, 741, 684 cm⁻¹; HRMS (ESI⁺) calculated for C₁₈H₁₂N₂O₃S [M+H]⁺, 337.0569; found 337.0637

(Z)-3-Benzyl-5-(1-methyl-2-oxoindolin-3-ylidene)thiazolidine-2,4-dione (5p)

Yield: 83%; Vermilion red solid; m.p: 186-188 °C; ¹H NMR (400 MHz, CDCl₃) δ 8.94 (d, *J* = 7.9 Hz, 1H, -H₄ of Indolin-2-one), 7.51 – 7.33 (m, 6H), 7.12 (t, *J* = 7.8 Hz, 1H, -H₆ of Indolin-2-one), 6.85 (d, *J* = 7.8 Hz, 1H, -H₇ of Indolin-2-one), 4.96 (s, 2H, -CH₂), 3.29 (s, 3H, -CH₃); ¹³C NMR (100 MHz, CDCl₃) δ 170.09, 167.38, 165.41, 144.95, 134.99, 132.53, 130.61, 128.98, 128.93, 128.80, 128.74, 128.72, 128.33, 127.43, 123.14, 119.80, 108.34, 44.88, 26.42; IR (ATR) ν 3852, 3741, 3614, 3031, 1746, 1663, 1522, 1465, 1376, 1332, 1148, 1064, 871, 749, 692 cm⁻¹; HRMS (ESI⁺) calculated for C₁₉H₁₄N₂O₃S [M+H]⁺, 351.0725; found 351.0796

(Z)-3-Benzyl-5-(1-ethyl-2-oxoindolin-3-ylidene)thiazolidine-2,4-dione (5q)

Yield: 78%; Vermilion red solid; m.p: 178-180 °C; ¹H NMR (400 MHz, CDCl₃) δ 8.98 (ddd, *J* = 7.9, 1.3, 0.5 Hz, 1H, -H₄ of Indolin-2-one), 7.50 – 7.28 (m, 6H), 7.13 (td, *J* = 7.8, 1.1 Hz, 1H, -H₆ of Indolin-2-one), 6.89 (ddd, *J* = 7.9, 1.1, 0.6 Hz, 1H, -H₇ of Indolin-2-

one), 4.97 (s, 2H, -CH₂), 3.85 (q, $J = 7.2$ Hz, 2H, -CH₂), 1.31 (t, $J = 7.2$ Hz, 3H, -CH₃); ¹³C NMR (100 MHz, CDCl₃) δ 170.16, 167.06, 165.47, 144.11, 135.01, 132.51, 130.49, 129.04, 128.98, 128.90, 128.87, 128.80, 128.63, 128.61, 128.49, 128.31, 127.64, 122.95, 120.05, 108.45, 44.85, 35.11, 12.75; IR (ATR) ν 3740, 1733, 1667, 1600, 1461, 1428, 1375, 1335, 1232, 1149, 1074, 1019, 748, 700 cm⁻¹; HRMS (ESI⁺) calculated for C₂₀H₁₆N₂O₃S [M+H]⁺, 365.0882; found 365.0948

(Z)-3-Benzyl-5-(1-benzyl-2-oxoindolin-3-ylidene)thiazolidine-2,4-dione (5r)

Yield: 72%; Vermilion red solid; m.p: 185-187 °C; ¹H NMR (400 MHz, CDCl₃) δ 9.01 (d, $J = 7.9$ Hz, 1H, -H₄ of Indolin-2-one), 7.49 (d, $J = 6.6$ Hz, 2H), 7.33 (ddt, $J = 15.5, 11.4, 6.1$ Hz, 9H), 7.13 (t, $J = 7.8$ Hz, 1H), 6.80 (d, $J = 7.9$ Hz, 1H), 5.01 (s, 2H, -CH₂), 4.99 (s, 2H, -CH₂); ¹³C NMR (100 MHz, CDCl₃) δ 170.00, 167.60, 165.46, 144.16, 135.07, 134.96, 132.52, 131.03, 128.91, 128.89, 128.87, 128.82, 128.33, 127.93, 127.40, 127.28, 123.20, 120.03, 109.36, 44.91, 44.12; IR (ATR) ν 3886, 2918, 2852, 1668, 1601, 1456, 1371, 1331, 1180, 1072, 1020, 963, 746, 697 cm⁻¹; HRMS (ESI⁺) calculated for C₂₅H₁₈N₂O₃S [M+H]⁺, 427.1038; found 427.1109

(Z)-3-benzyl-5-(1-(4-chlorobenzyl)-2-oxoindolin-3-ylidene)thiazolidine-2,4-dione (5s)

Yield: 67%; Vermilion red solid; m.p: 185-188 °C; ¹H NMR (400 MHz, CDCl₃) δ 9.02 (d, $J = 7.9$, 1H, -H₄ of Indolin-2-one), 7.55 – 7.45 (m, 4H), 7.40 – 7.28 (m, 4H), 7.20 – 7.03 (m, 3H), 6.79 – 6.75 (m, 1H), 5.03 (d, $J = 13.0$ Hz, 4H, -CH₂); ¹³C NMR (100 MHz, CDCl₃) δ 169.74, 167.53, 165.39, 147.78, 134.86, 134.22, 132.52, 132.03, 131.33, 129.30, 128.89, 128.83, 128.41, 127.03, 123.39, 121.94, 120.84, 109.05, 45.25, 43.54; IR (ATR) ν 3780, 1736, 1666, 1602, 1467, 1340, 1184, 1143, 1073, 1021, 872, 749, 690 cm⁻¹; HRMS (ESI⁺) calculated for C₂₅H₁₇ClN₂O₃S [M+H]⁺, 461.0648; found 461.0720

(Z)-3-Benzyl-5-(1-(4-bromobenzyl)-2-oxoindolin-3-ylidene)thiazolidine-2,4-dione (5t)

Yield: 68%; Vermilion red solid; mp = 170-173 °C; ¹H NMR (400 MHz, CDCl₃) δ 9.01 (dd, $J = 7.9, 1.2$ Hz, 1H, -H₄ of Indolin-2-one), 7.52 – 7.44 (m, 4H), 7.40 – 7.31 (m, 4H), 7.23 – 7.09 (m, 3H), 6.79 – 6.72 (m, 1H), 4.97 (d, $J = 13.0$ Hz, 4H, -CH₂); ¹³C NMR (100 MHz, CDCl₃) δ 169.84, 167.57, 165.39, 143.78, 134.93, 134.12, 132.52, 132.08, 131.33, 129.00, 128.89, 128.83, 128.37, 127.13, 123.39, 121.94, 120.04, 109.15, 44.95, 43.54; IR (ATR) ν 3781, 3705, 2356, 1666, 1602, 1476, 1344, 1184, 1143, 1073, 1011, 960, 872,

749, 693 cm^{-1} ; HRMS (ESI⁺) calculated for $\text{C}_{25}\text{H}_{17}\text{BrN}_2\text{O}_3\text{S}$ [M+H]⁺, 505.0143; found 505.0217

***(Z)*-3-Benzyl-5-(1-(4-nitrobenzyl)-2-oxoindolin-3-ylidene)thiazolidine-2,4-dione (5u)**

Yield: 65%; Vermilion red solid; m.p: 220-222 °C; ¹H NMR (400 MHz, CDCl_3) δ 9.04 (d, $J = 7.9$ Hz, 1H, -H₄ of Indolin-2-one), 8.20 (d, $J = 8.3$ Hz, 2H), 7.52 – 7.43 (m, 4H), 7.35 (t, $J = 7.9$ Hz, 4H), 7.17 (t, $J = 7.8$ Hz, 1H), 6.72 (d, $J = 7.8$ Hz, 1H), 5.10 (s, 2H, -CH₂), 4.98 (s, 2H, -CH₂); ¹³C NMR (100 MHz, CDCl_3) δ 169.60, 167.62, 165.31, 147.72, 143.34, 142.42, 134.86, 132.57, 131.88, 129.19, 128.98, 128.91, 128.84, 128.41, 128.02, 126.74, 124.22, 123.70, 120.09, 108.85, 45.01, 43.48; IR (ATR) ν 3779, 1742, 1672, 1605, 1518, 1467, 1340, 1190, 1137, 1082, 1031, 873, 746, 690 cm^{-1} ; HRMS (ESI⁺) calculated for $\text{C}_{25}\text{H}_{17}\text{N}_3\text{O}_5\text{S}$ [M+H]⁺, 472.0889; found 472.0967

***(Z)*-3-(4-Chlorobenzyl)-5-(2-oxoindolin-3-ylidene)thiazolidine-2,4-dione (5v)**

Yield: 55%; Vermilion red solid; m.p: 230-231 °C; ¹H NMR (400 MHz, $\text{DMSO}-d_6$) δ 11.27 (s, 1H), 8.83 – 8.76 (m, 1H), 7.45 – 7.36 (m, 5H), 7.10 (td, $J = 7.7, 1.1$ Hz, 1H), 6.97 (d, $J = 7.7$ Hz, 1H), 4.87 (s, 2H, -CH₂ attached to TZD); ¹³C NMR (100 MHz, $\text{DMSO}-d_6$) δ 170.57, 168.77, 165.89, 144.47, 134.83, 133.37, 132.90, 130.21, 130.01, 129.07, 128.44, 127.81, 122.60, 120.30, 111.06, 44.06; IR (ATR) ν 3778, 3706, 3189, 2794, 2356, 1744, 1666, 1614, 1388, 1335, 1232, 1149, 1089, 755, 676 cm^{-1} ; HRMS (ESI⁺) calculated for $\text{C}_{18}\text{H}_{11}\text{ClN}_2\text{O}_3\text{S}$ [M+H]⁺, 371.0179; found 371.0226

***(Z)*-3-(4-Chlorobenzyl)-5-(1-methyl-2-oxoindolin-3-ylidene)thiazolidine-2,4-dione (5w)**

Yield: 63%; Vermilion red solid; m.p: 240-241 °C; ¹H NMR (400 MHz, CDCl_3) δ 9.00 – 8.93 (m, 1H), 7.50 – 7.30 (m, 5H), 7.16 (td, $J = 7.8, 1.1$ Hz, 1H, -H₆ of Indolin-2-one), 6.90 (d, $J = 7.8$ Hz, 1H, -H₇ of Indolin-2-one), 4.93 (s, 2H, -CH₂ attached to TZD), 3.32 (s, 3H, -CH₃); ¹³C NMR (100 MHz, CDCl_3) δ 170.09, 167.40, 165.39, 145.05, 134.38, 133.40, 132.70, 130.43, 130.33, 129.00, 128.78, 127.74, 123.20, 119.81, 108.41, 44.16, 26.45; IR (ATR) ν 3778, 3704, 2917, 2850, 2356, 1729, 1660, 1600, 1470, 1431, 1375, 1145, 1063, 867, 799, 750 cm^{-1} ; HRMS (ESI⁺) calculated for $\text{C}_{19}\text{H}_{13}\text{ClN}_2\text{O}_3\text{S}$ [M+H]⁺, 385.0335; found 385.0390.

***(Z)*-3-(4-Chlorobenzyl)-5-(1-ethyl-2-oxoindolin-3-ylidene)thiazolidine-2,4-dione (5x)**

Yield: 68%; Vermilion red solid; m.p: 248-251 °C; ¹H NMR (400 MHz, CDCl₃) δ 9.02 – 8.94 (m, 1H), 7.49 – 7.38 (m, 3H), 7.38 – 7.29 (m, 2H), 7.16 (td, *J* = 7.8, 1.1 Hz, 1H, -H₆ of Indolin-2-one), 6.91 (d, *J* = 7.8 Hz, 1H, -H₇ of Indolin-2-one), 4.93 (s, 2H, -CH₂ attached to TZD), 3.87 (q, *J* = 7.2 Hz, 2H, -CH₂ attached to Indolin-2-one), 1.32 (t, *J* = 7.2 Hz, 3H, -CH₃). ¹³C NMR (100 MHz, CDCl₃) δ 170.16, 167.05, 165.43, 144.20, 134.36, 133.42, 132.66, 130.38, 129.00, 127.93, 123.00, 120.03, 108.51, 44.13, 35.13, 12.73; IR (ATR) ν 3875, 3780, 3704, 2356, 1723, 1643, 1307, 1057, 796, 749 cm⁻¹; HRMS (ESI⁺) calculated for C₂₀H₁₅ClN₂O₃S [M+H]⁺, 399.0492; found 399.0544.

***(Z)*-5-(1-Benzyl-2-oxoindolin-3-ylidene)-3-(4-chlorobenzyl)thiazolidine-2,4-dione (5y)**

Yield: 72%; Vermilion red solid; m.p: 318-320 °C; ¹H NMR (400 MHz, CDCl₃) δ 8.99 (dd, *J* = 8.0, 1.2 Hz, 1H, -H₄ of Indolin-2-one), 7.47 – 7.38 (m, 2H), 7.38 – 7.25 (m, 8H), 7.14 (td, *J* = 7.8, 1.1 Hz, 1H, -H₆ of Indolin-2-one), 6.81 (d, *J* = 7.9 Hz, 1H, -H₇ of Indolin-2-one), 5.01 (s, 2H, -CH₂ attached to TZD), 4.95 (s, 2H, -CH₂ attached to Indolin-2-one); ¹³C NMR (100 MHz, CDCl₃) δ 170.00, 167.55, 165.39, 144.22, 135.02, 134.39, 133.39, 132.65, 130.40, 129.01, 128.93, 128.88, 127.95, 127.63, 127.28, 123.23, 119.99, 109.41, 44.18, 29.71; IR (ATR) ν 3778, 3703, 2920, 2854, 2356, 1733, 1668, 1602, 1457, 1353, 1262, 1162, 1074, 1017, 870, 798, 740 cm⁻¹; HRMS (ESI⁺) calculated for C₂₅H₁₇ClN₂O₃S [M+H]⁺, 461.0648; found 461.0695.

***(Z)*-3-(4-chlorobenzyl)-5-(1-(4-chlorobenzyl)-2-oxoindolin-3-ylidene)thiazolidine-2,4-dione (5z)**

Yield: 70%; Vermilion red solid; m.p: 220-222 °C; ¹H NMR (400 MHz, CDCl₃) δ 9.06 – 8.99 (m, 1H), 8.25 – 8.17 (m, 2H), 7.51 – 7.41 (m, 4H), 7.40 – 7.32 (m, 3H), 7.18 (td, *J* = 7.8, 1.1 Hz, 1H, -H₆ of Indolin-2-one), 6.73 (dt, *J* = 7.8, 0.9 Hz, 1H, -H₇ of Indolin-2-one), 5.11 (s, 2H, -CH₂ attached to TZD), 4.95 (s, 2H, -CH₂ attached to Indolin-2-one); ¹³C NMR (100 MHz, CDCl₃) δ 169.60, 167.59, 165.26, 147.74, 143.40, 142.36, 134.47, 133.28, 132.70, 131.56, 130.43, 129.19, 129.04, 128.02, 126.99, 124.24, 123.74, 120.06, 108.90, 44.28, 43.49; IR (ATR) ν 3779, 3706, 2356, 1734, 1663, 1600, 1513, 1468, 1340, 1164, 1082, 1024, 868, 798, 744 cm⁻¹; HRMS (ESI⁺) calculated for C₂₅H₁₆Cl₂N₂O₃S [M+H]⁺, 494.0259; found 494.0253.

***(Z)*-3-(4-chlorobenzyl)-5-(1-(4-nitrobenzyl)-2-oxoindolin-3-ylidene)thiazolidine-2,4-dione (5aa)**

Yield: 68%; Vermilion red solid; m.p: 230-232 °C; ¹H NMR (400 MHz, CDCl₃) δ 9.06 (d, *J* = 7.9 Hz, 1H, -H₄ of Indolin-2-one), 8.23 (d, *J* = 8.3 Hz, 2H), 7.51 – 7.41 (m, 4H), 7.35 (t, *J* = 7.9 Hz, 4H), 7.18 (t, *J* = 7.8 Hz, 1H), 6.73 (d, *J* = 7.8 Hz, 1H), 5.11 (s, 2H, -CH₂), 4.96 (s, 2H, -CH₂); ¹³C NMR (100 MHz, CDCl₃) δ 169.60, 167.52, 165.31, 147.72, 143.44, 142.42, 134.86, 132.57, 131.88, 129.19, 128.98, 128.91, 128.84, 128.41, 128.02, 126.74, 124.22, 123.70, 120.09, 108.85, 45.01, 43.48; IR (ATR) ν 3779, 2536, 1742, 1672, 1600, 1518, 1467, 1340, 1190, 1137, 1085, 1031, 868, 756, 690 cm⁻¹; HRMS (ESI⁺) calculated for C₂₅H₁₆ClN₃O₅S [M+H]⁺, 506.0499; found 506.0522

***(Z)*-3-(4-Bromobenzyl)-5-(2-oxoindolin-3-ylidene)thiazolidine-2,4-dione (5ab)**

Yield: 58%; Vermilion red solid; m.p: 225-228 °C; ¹H NMR (400 MHz, DMSO-*d*₆) δ 11.27 (s, 1H, -NH), 8.79 (d, *J* = 7.9 Hz, 1H, -H₄ of Indolin-2-one), 7.60 – 7.49 (m, 2H), 7.42 (td, *J* = 7.7, 1.2 Hz, 1H, -H₅ of Indolin-2-one), 7.33 (d, *J* = 8.3 Hz, 2H), 7.09 (t, *J* = 7.7 Hz, 1H, -H₆ of Indolin-2-one), 6.97 (d, *J* = 7.8 Hz, 1H, -H₇ of Indolin-2-one), 4.85 (s, 2H, -CH₂ attached to TZD); ¹³C NMR (100 MHz, DMSO-*d*₆) δ 170.56, 168.76, 165.88, 144.47, 135.24, 133.37, 131.99, 130.54, 129.99, 128.44, 127.82, 122.59, 121.43, 120.29, 111.06, 44.12; IR (ATR) ν 3777, 3383, 2357, 1666, 1457, 1387, 1336, 1233, 991, 829, 758 cm⁻¹; HRMS (ESI⁺) calculated for C₁₈H₁₁BrN₂O₃S [M+H]⁺, 414.9674; found 414.9715.

***(Z)*-3-(4-Bromobenzyl)-5-(1-methyl-2-oxoindolin-3-ylidene)thiazolidine-2,4-dione (5ac)**

Yield: 63%; Vermilion red solid; m.p: 235-238 °C; ¹H NMR (400 MHz, CDCl₃) δ 8.94 (dd, *J* = 8.0, 1.2 Hz, 1H, -H₄ of Indolin-2-one), 7.54 – 7.42 (m, 3H), 7.39 – 7.27 (m, 2H), 7.18 – 7.11 (m, 1H), 6.89 (d, *J* = 7.8 Hz, 1H, -H₇ of Indolin-2-one), 4.91 (s, 2H, -CH₂ attached to TZD), 3.31 (s, 3H, -CH₃ attached to Indolin-2-one); ¹³C NMR (100 MHz, CDCl₃) δ 170.09, 167.39, 165.37, 145.05, 133.90, 132.71, 131.97, 130.73, 128.78, 123.20, 122.54, 119.80, 108.42, 44.21, 26.45; IR (ATR) ν 3779, 3707, 3189, 2356, 1661, 1597, 1478, 1334, 1146, 1062, 1014, 862, 795, 753 cm⁻¹; HRMS (ESI⁺) calculated for C₁₉H₁₃BrN₂O₃S [M+H]⁺, 428.9830; found 428.9861.

***(Z)*-3-(4-Bromobenzyl)-5-(1-ethyl-2-oxoindolin-3-ylidene)thiazolidine-2,4-dione (5ad)**

Yield: 67%; Vermilion red solid; m.p: 350-352 °C; ¹H NMR (400 MHz, CDCl₃) δ 8.97 (dd, *J* = 7.9, 1.2 Hz, 1H, -H₄ of Indolin-2-one), 7.53 – 7.40 (m, 3H), 7.40 – 7.28 (m, 2H),

Chapter V

7.15 (td, $J = 7.7, 1.0$ Hz, 1H, -H₆ of Indolin-2-one), 6.91 (d, $J = 7.9$ Hz, 1H, -H₇ of Indolin-2-one), 4.91 (s, 2H, -CH₂ attached to TZD), 3.86 (q, $J = 7.2$ Hz, 2H, -CH₂ attached to Indolin-2-one), 1.32 (t, $J = 7.2$ Hz, 3H, -CH₃); ¹³C NMR (100 MHz, CDCl₃) δ 170.15, 167.03, 165.40, 144.19, 133.92, 132.66, 131.96, 130.69, 130.14, 128.98, 127.91, 122.99, 122.51, 120.02, 108.51, 44.18, 35.13, 12.74; IR (ATR) ν 3778, 3706, 2356, 1667, 1596, 1470, 1427, 1373, 1330, 1233, 1148, 1070, 1011, 871, 842, 794, 753 cm⁻¹; HRMS (ESI⁺) calculated for C₂₀H₁₅BrN₂O₃S [M+H]⁺, 442.9987; found 443.0021.

(Z)-5-(1-Benzyl-2-oxoindolin-3-ylidene)-3-(4-bromobenzyl)thiazolidine-2,4-dione (5ae)

Yield: 69%; Vermilion red solid; m.p: 228-230 °C; ¹H NMR (400 MHz, CDCl₃) δ 8.98 (d, $J = 7.9$ Hz, 1H, -H₄ of Indolin-2-one), 7.53 – 7.44 (m, 3H), 7.39 – 7.31 (m, 7H), 7.29 – 7.09 (m, 2H), 6.81 (d, $J = 7.9$ Hz, 1H, -H₇ of Indolin-2-one), 5.01 (s, 2H, -CH₂ attached to Indolin-2-one), 4.93 (s, 2H, -CH₂ attached to TZD); ¹³C NMR (100 MHz, CDCl₃) δ 169.99, 167.55, 165.38, 144.23, 135.02, 133.89, 132.66, 131.98, 130.69, 128.92, 128.88, 127.95, 127.65, 127.28, 123.23, 122.54, 119.99, 109.41, 44.23, 44.14; IR (ATR) ν 3781, 3706, 2919, 2853, 2356, 1729, 1664, 1598, 1455, 1153, 1067, 962, 869, 794, 736 cm⁻¹; HRMS (ESI⁺) calculated for C₂₅H₁₇BrN₂O₃S [M+H]⁺, 505.0143; found 505.0170.

(Z)-3-(4-bromobenzyl)-5-(1-(4-chlorobenzyl)-2-oxoindolin-3-ylidene)thiazolidine-2,4-dione (5af)

Yield: 63%; Vermilion red solid; m.p: 230-232 °C; ¹H NMR (400 MHz, CDCl₃) δ 9.02 (dd, $J = 8.0, 1.2$ Hz, 1H, -H₄ of Indolin-2-one), 8.27 – 8.17 (m, 2H), 7.54 – 7.43 (m, 4H), 7.42 – 7.33 (m, 3H), 7.18 (td, $J = 7.8, 1.0$ Hz, 1H, -H₆ of Indolin-2-one), 6.73 (d, $J = 7.8$ Hz, 1H, -H₇ of Indolin-2-one), 5.11 (s, 2H, -CH₂ attached to Indolin-2-one), 4.93 (s, 2H, -CH₂ attached to TZD); ¹³C NMR (100 MHz, CDCl₃) δ 169.58, 167.59, 165.24, 147.75, 143.41, 142.36, 133.78, 132.70, 132.01, 131.53, 130.72, 129.19, 128.02, 127.00, 124.23, 123.73, 122.62, 120.06, 108.90, 44.34, 43.50; IR (ATR) ν 3780, 3706, 2356, 1661, 1598, 1514, 1467, 1337, 870, 794, 750 cm⁻¹; HRMS (ESI⁺) calculated for C₂₅H₁₆BrClN₂O₃S [M+H]⁺, 538.9754; found 538.9797.

(Z)-3-(4-bromobenzyl)-5-(1-(4-nitrobenzyl)-2-oxoindolin-3-ylidene)thiazolidine-2,4-dione (5ag)

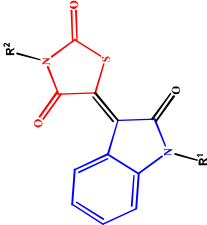
Yield: 62%; Vermilion red solid; m.p: 225-227 °C; ¹H NMR (400 MHz, CDCl₃) δ 9.06 (d, $J = 7.9$ Hz, 1H, -H₄ of Indolin-2-one), 8.22 (d, $J = 8.3$ Hz, 2H), 7.52 – 7.43 (m, 4H), 7.35

(t, $J = 7.9$ Hz, 4H), 7.17 (t, $J = 7.8$ Hz, 1H), 6.72 (d, $J = 7.8$ Hz, 1H), 5.10 (s, 2H, $-\text{CH}_2$), 4.98 (s, 2H, $-\text{CH}_2$); ^{13}C NMR (100 MHz, CDCl_3) δ 169.60, 167.62, 165.31, 147.72, 143.34, 142.42, 134.86, 132.57, 131.88, 129.19, 128.98, 128.91, 128.84, 128.41, 128.02, 126.74, 124.22, 123.70, 120.09, 108.85, 45.01, 43.48; IR (ATR) ν 3779, 2542, 1742, 1672, 1605, 1518, 1469, 1350, 1190, 1139, 1082, 1033, 870, 746, 693 cm^{-1} ; HRMS (ESI⁺) calculated for $\text{C}_{25}\text{H}_{16}\text{BrN}_3\text{O}_5\text{S}$ $[\text{M}+\text{H}]^+$, 538.9754.; found 538.9778

5.3. PL inhibition assay, enzyme kinetics and structural activity relationship

The *in-vitro* PL inhibitory activity of the synthesized analogues was evaluated by a standardised assay protocol [14,21]. The assay protocol consisted of Porcine PL Type II (enzyme), 4-nitrophenyl butyrate (substrate) and orlistat (standard). Stock solutions of the synthesized analogues were prepared in DMSO at linear concentrations ranging from 1.56 - 2000 $\mu\text{g}/\text{mL}$. Amount of the *p*-nitrophenol released by the PL was measured at its maximum wavelength (405 nm). As summarised in **Table 5.1**, synthesized analogues displayed potential to moderate PL inhibition ($\text{IC}_{50} = 7.30$ to 43.20 μM). Orlistat exhibited a potent PL inhibitory activity ($\text{IC}_{50} = 0.86$ μM). Most of the analogues exhibited good (< 15 μM) to moderate (15-30 μM) activity, while few analogues displayed poor activity (> 30 μM). Analogue **5r** exhibited the most potential activity against PL, with an IC_{50} of 7.30 μM , followed by **5t** ($\text{IC}_{50} = 9.51$ μM).

To study the inhibition mode against the PL, enzyme inhibition kinetics analysis of the topmost active analogues (**5r** and **5t**) was performed. The inhibition type can be deduced from the Lineweaver–Burk (LB) plots [22]. A LB plot was constructed by performing an *in-vitro* PL inhibition assay, wherein various concentrations of the analogues were evaluated against the different concentrations of the substrate (25, 50, 100 and 200 μM). The obtained LB plots were converged at its first quadrant that intersected at one point, indicating that the analogues **5r** and **5t** inhibited PL in a competitive manner (**Fig. 5.4**). A proportionate increase in the apparent K_m values without affecting the V_{max} further indicated the scope of a reversible competitive inhibition (**Table 5.2**). Inhibition constant (K_i) values were deduced as 4.637 and 6.041 μM (retrieved from the Cheng-Prusoff equation [23]), proving that these molecules have a moderate affinity towards PL. Orlistat exerted a K_i value of 0.528 μM with a competitive mode of enzyme inhibition. From the enzyme kinetics study, it can be concluded that the synthesized analogues were bound to the active site of the PL during the inhibition.

Table 5.1 *In-vitro* PL inhibitory activity of the synthesized analogues (5a-5ag)


#	R ¹	R ²	IC ₅₀ (μ M)*	#	R ¹	R ²	IC ₅₀ (μ M)*
5a	H	Methyl	28.37 \pm 1.42	5r	Benzyl	Benzyl	7.30 \pm 0.80
5b	Methyl	Methyl	18.43 \pm 0.39	5s	4-Chlorobenzyl	Benzyl	11.70 \pm 1.66
5c	Ethyl	Methyl	21.79 \pm 1.98	5t	4-Bromobenzyl	Benzyl	9.51 \pm 1.19
5d	Benzyl	Methyl	12.22 \pm 1.21	5u	4-Nitrobenzyl	Benzyl	12.27 \pm 1.38
5e	4-Chlorobenzyl	Methyl	14.19 \pm 0.53	5v	H	4-Chlorobenzyl	27.85 \pm 2.05
5f	4-Bromobenzyl	Methyl	12.10 \pm 1.25	5w	Methyl	4-Chlorobenzyl	21.71 \pm 0.62
5g	4-Nitrobenzyl	Methyl	17.06 \pm 1.06	5x	Ethyl	4-Chlorobenzyl	24.88 \pm 1.80
5h	H	Ethyl	35.50 \pm 1.94	5y	Benzyl	4-Chlorobenzyl	11.36 \pm 1.08
5i	Methyl	Ethyl	17.29 \pm 1.59	5z	4-Chlorobenzyl	4-Chlorobenzyl	25.48 \pm 0.67
5j	Ethyl	Ethyl	15.42 \pm 0.74	5aa	4-Nitrobenzyl	4-Chlorobenzyl	31.58 \pm 0.99
5k	Benzyl	Ethyl	12.29 \pm 1.55	5ab	H	4-Bromobenzyl	24.00 \pm 2.17
5l	4-Bromobenzyl	Ethyl	14.14 \pm 1.46	5ac	Methyl	4-Bromobenzyl	13.60 \pm 1.62
5m	4-Chlorobenzyl	Ethyl	19.64 \pm 1.83	5ad	Ethyl	4-Bromobenzyl	18.49 \pm 2.06
5n	4-Nitrobenzyl	Ethyl	20.78 \pm 0.71	5ae	Benzyl	4-Bromobenzyl	11.87 \pm 0.83
5o	H	Benzyl	26.61 \pm 1.34	5af	4-Chlorobenzyl	4-Bromobenzyl	12.57 \pm 1.46
5p	Methyl	Benzyl	14.65 \pm 1.53	5ag	4-Nitrobenzyl	4-Bromobenzyl	43.20 \pm 1.49
5q	Ethyl	Benzyl	17.46 \pm 1.22	Orlistat	---	---	0.86 \pm 0.11

* All the experiments were performed in triplicate and the values are represented as mean \pm S.E.M

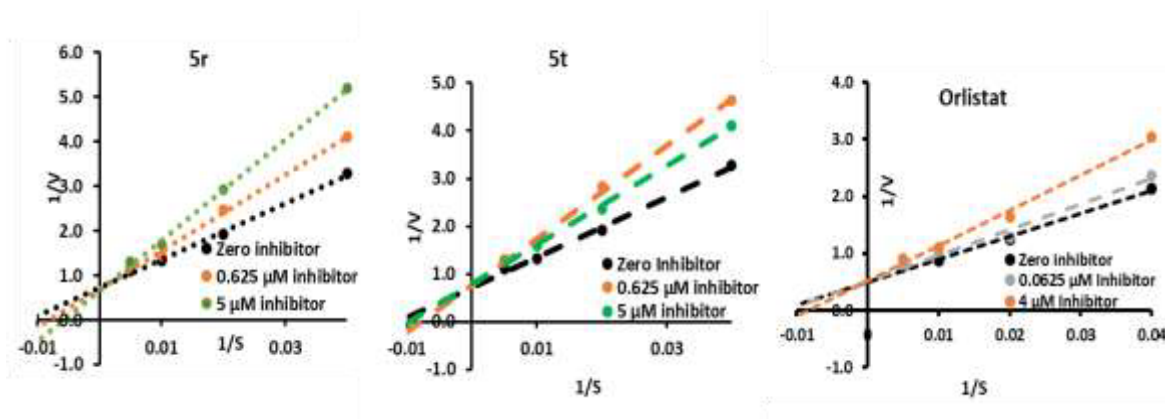


Fig. 5.4. Double reciprocal Lineweaver-Burk plots of analogues **5r**, **5t** and **orlistat**

Table 5.2. K_m , V_{max} and K_i values of **5r** and **5t** retrieved from the PL enzyme kinetics.

Code	K_m (apparent) at different concentration (μM)			V_{max} ($\mu\text{M}/\text{min}$)	K_i (μM)	Nature of inhibition
	0 μM	0.625 μM	5 μM			
5r	87.053	121.438	170.487	1.439	4.637	Competitive
5t	87.053	103.378	127.486	1.316	6.041	Competitive
Orlistat	79.757	87.301 [@]	119.756 ^{&}	1.956	0.528	Competitive

[@]0.0625 μM ; [&]4 μM orlistat concentration

Based on the *in-vitro* PL inhibition assay, a preliminary structure-activity relationship of the screened analogues was deduced. The PL inhibitory potential of the analogues varied with respect to the substitutions on the isatin and imide nitrogen of TZD. Substitution of TZD with alkyl functionalities resulted in analogues **5a** to **5n**, that exhibited a lesser PL inhibition than the aryl functionalities (**5o** to **5ag**). For instance, analogue **5r** exhibited a significant PL inhibitory potential ($\text{IC}_{50} = 7.30 \mu\text{M}$) than the analogues **5d** and **5k**, that lacked benzyl extension on the TZD scaffold ($\text{IC}_{50} = 12.22$ and $12.29 \mu\text{M}$, respectively). Furthermore, the substitution of the electron withdrawing substituents resulted in the reduction of the PL inhibitory activity. Analogue **5y** with a 4-chlorobenzyl substituent on imidic nitrogen exhibited a weaker PL inhibition ($\text{IC}_{50} = 11.36 \mu\text{M}$) than the **5r** that lacked such electron withdrawing groups on the aromatic functionality ($\text{IC}_{50} = 7.30 \mu\text{M}$). The presence of substitution on the isatin nitrogen increased the PL inhibitory activity. Unsubstituted hybrid analogues (**5a**, **5h**, **5o**, **5v** and **5ab**) exhibited a moderate to poor inhibitory potential towards the PL ($\text{IC}_{50} = 28.37$ and $35.50 \mu\text{M}$, respectively).

Chapter V

Introduction of bulkier aromatic substitutions resulted in the enhancement of PL inhibitory potential.

However, this trend depends on the substitutions of the bulkier aromatic functionalities. For instance, among the various substitutions, p-NO₂ counterpart (analogues **5g**, **5n**, **5u**, **5aa** and **5ag**) displayed a comparatively lesser activity (IC₅₀ = 17.06, 20.78, 12.27, 31.58 and 43.20 μM, respectively) than the unsubstituted benzyl part (analogues **5d**, **5k**, **5r**, **5y** and **5ae** with an IC₅₀ of 12.22, 12.29, 7.30, 11.36 and 11.87 μM, respectively). Further, -Br substituted analogues (**5f** and **5t**) exhibited comparatively higher activity (IC₅₀ = 12.10 and 9.51 μM, respectively) than the -Cl substituted analogues (**5e** and **5s**; IC₅₀ = 14.19 and 11.70 μM, respectively). Based on these observations, a preliminary structural activity relationship was deduced and is represented in **Fig. 5.5**.

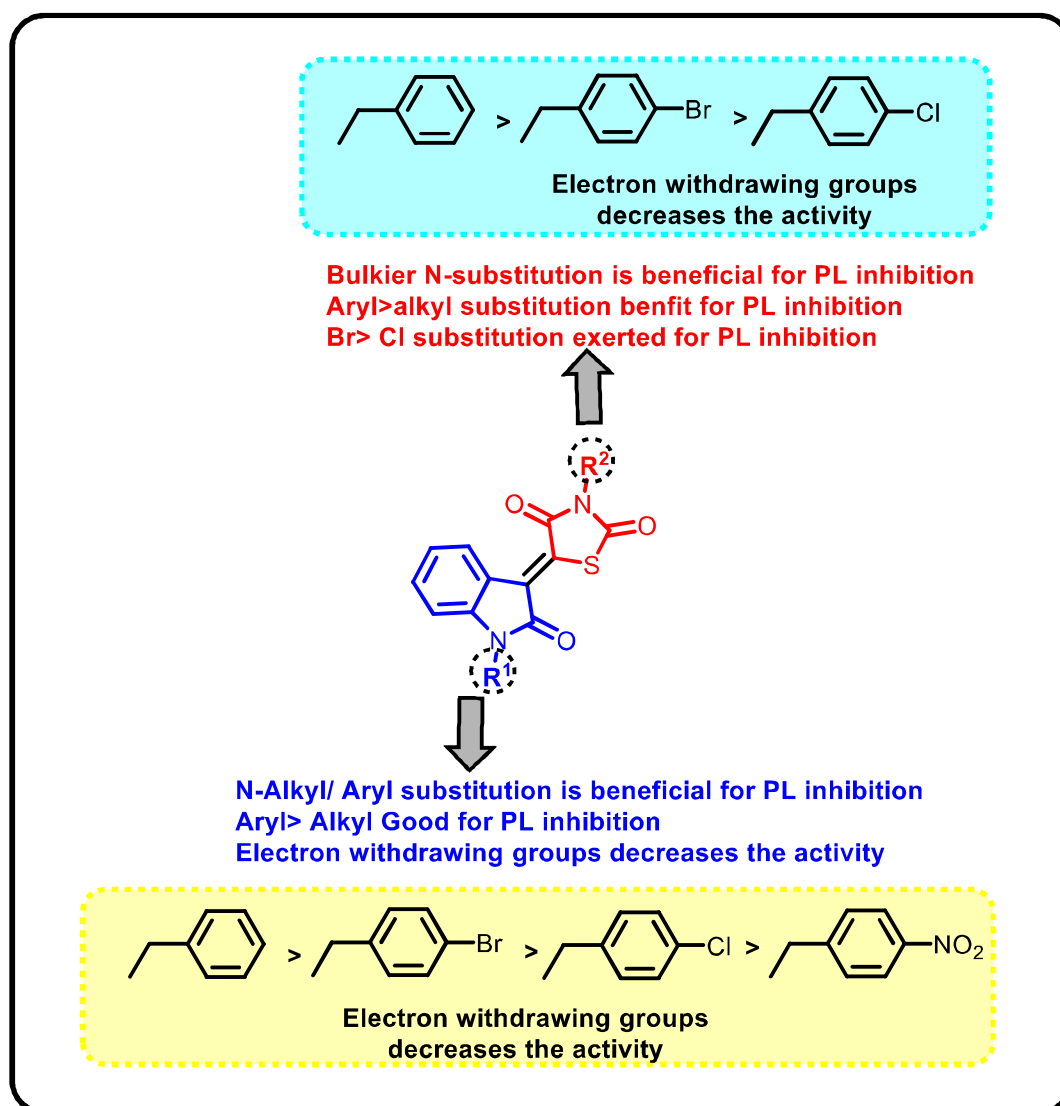


Fig. 5.5. Structure–activity relationship of synthesized Indole-TZD hybrid analogues (**5a-5ag**)

5.4. Fluorescence Quenching Measurements with PL

The fluorescence property of PL is originated from various aromatic amino acids such as tryptophan (Trp), phenylalanine (Phe) and tyrosine (Tyr). PL possesses 25 Phe residues, 16 Tyr residues and 7 Trp residues, that may account for fluorescence emission. The quantum yield for Phe is very low; thus, the intrinsic fluorescence is mainly contributed by the Trp residues (Trp 17, Trp 30, Trp 86, Trp 107, Trp 253, Trp 339, and Trp 403) only. Further, changes in emission spectra of tryptophan is observed with the various structural and dynamic properties of a macromolecule. Thus, the association reaction between a bioactive analogue with a PL can be investigated by using intrinsic fluorescence spectroscopy [24,25].

The effects of the synthesized analogues (**5r** and **5t**) on the fluorescence quenching of PL were evaluated by the previously reported method with the necessary modifications [25] and the results are summarised in **Fig. 5.6**.

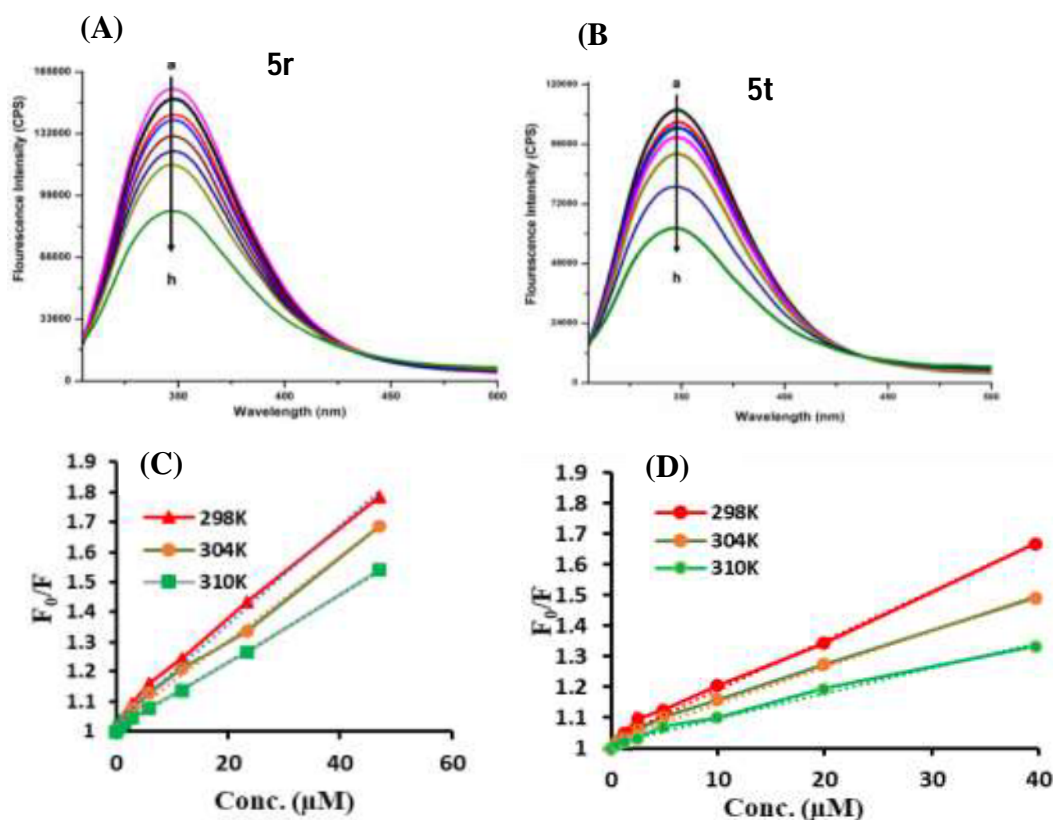


Fig. 5.6. (A), (B) The fluorescence spectra of PL in the presence of **5r** and **5t** at various concentrations (pH 7.4, T = 298 K, a to h in increasing concentrations); (C), (D) Stern–Volmer plots for the quenching of **5r** and **5t** on the PL at 300 K

Chapter V

As shown in **Fig. 5.6**, the analogues (**5r** and **5t**) exerted a quenching effect on the PL fluorescence. Moreover, the fluorescence intensity was decreased with the increase in the quencher (**5r** and **5t**) concentration indicating the formation of PL-quencher complexes.

Fluorescence quenching is classified into two types, namely static quenching and dynamic quenching. When the excited state fluorophore is deactivated by the quencher molecule in solution it is denoted as dynamic quenching, while the formation of a non-fluorescent ground state complex of fluorophores -quencher is described as static quenching. A direct correlation between quenching constant and the temperature highlights the dynamic quenching, while a diminished quenching constant with increase in temperature represents static quenching [26,27].

Fluorescence quenching is described by the Stern– Volmer equation as follows:

$$\frac{F_0}{F} = 1 + K_q \tau_0 [Q] = 1 + K_{SV} [Q] \dots\dots\dots \text{Formula 5.1}$$

where F and F_0 are the fluorescence intensities of PL with or without quencher, respectively. $[Q]$ represents the concentration of the quencher. K_{sv} denotes the Stern–Volmer quenching constant, while K_q is the bimolecular quenching constant, τ_0 is the average lifetime of the fluorophore molecule without quencher (10^{-8} s). The values of K_{sv} , K_q are determined from the linear regression plot of F_0/F Vs $[Q]$.

As represented in **Table 5.3**, an inverse correlation between the K_{sv} and temperature suggested that the quenching effects on the PL may be mainly attributed due to static quenching rather than dynamic quenching. A similar kind of result was previously reported by Yan-Qin Li *et al.*, wherein quercetin, isoquercetin, rutin exhibited an inverse correlation with the temperature and fluorescence intensity of the PL. The term K_q reflects the quenching efficiency or accessibility of fluorophore by the quencher; thus, it provides information about the formation of the complex. The K_q value near to $1 \times 10^{10} \text{ M}^{-1} \text{ s}^{-1}$ is typical for dynamic quenching. In the present study, K_q values were 52 to 103-fold higher ($10^{10} \text{ M}^{-1} \text{ s}^{-1}$) than dynamic quenching, thus suggesting that both analogues (**5r** and **5t**) formed a complex with PL, thereby quenching the fluorescence intensity *via* static mechanism [24,28].

For static quenching, binding constant and number of binding sites were calculated by the modified Stern– Volmer equation as follows.

Chapter V

$$\log \frac{F_0}{F} = \log K_b + n \log [Q] \dots\dots\dots \text{Formula 5.2}$$

where, K_b is the binding constant and n is the number of binding sites. Values of these parameters were determined from the double log graph of $\log F_0/F$ Vs $\log [Q]$. [28] The obtained values of these parameters are represented in **Table 5.3**

Table 5.3. Bimolecular quenching constant (K_q), binding constant (K_b) and the number of binding sites (n) at different temperatures for with **5r** and **5t**

#	T (K)	K_{sv} ($\times 10^4 M^{-1}$)	K_q ($\times 10^{10} M^{-1} s^{-1}$)	R^2	K_b ($\times 10^4 M^{-1} s^{-1}$)	n	R^2
5r	298	1.6	103.14	0.9920	3.22	0.841	0.9898
	304	1.4	88.68	0.9941	2.82	0.822	0.9933
	310	1.1	71.07	0.9992	2.00	0.822	0.9937
5t	298	1.6	101.13	0.9936	3.94	0.717	0.9868
	304	1.2	75.47	0.9921	3.03	0.747	0.9992
	310	0.8	52.20	0.9908	1.79	0.787	0.9945

The values of “ n ” at the corresponding temperature were in the range of 0.717 to 0.841, that indicated the presence of only one binding site in PL. This result further supported the competitive inhibition on the enzyme kinetics of PL. Additionally, the “ K_b ” values were in the range of 1.79 to $3.22 \times 10^4 M^{-1} s^{-1}$ indicating the strong binding forces of these analogues with PL.

5.5. Molecular docking and Dynamics

To decipher the degree of energetics and structural interactions, mechanism responsible for the PL inhibition and the binding mode of the analogues, molecular docking simulations were performed. All the synthesized analogues were docked in the crystal structure of PL-Colipase complex (PDB ID: 1LPB, 2.46 Å resolution) *via* Molegro Virtual Docker 6.0 [29] with validated grid parameters[14,17] and the obtained results are summarised in **Table 5.4.** and **Fig. 5.7.** The MolDock scores of all the analogues exhibited significant correlation to their PL inhibitory activity (Pearson’s $r = 0.8251$, $p < 0.05$) and these activities were exerted by *via* various interactions such as hydrogen bonding, π - π stacking, π -sulfur, π -cation and π -sigma etc. The most active analogue (**5r**) from the series possessed a top docking score of -99.740 kcal/mol, while **5t**, the second most active in the series, exhibited a MolDock score of -94.850 kcal/mol. All the analogues interacted with the hydrophobic lid domain (Phe 77, Phe 215) as well as the catalytic triad amino acids (Ser 152, His 263)

Chapter V

Table 5.4. Mol Dock scores (in kcal/ mol) and the interaction summary of the synthesized analogues (5a- 5ag) with the human PL active site of ILPB

#	Mol Dock Score	H-bond	π - π interaction	π -cation	Alkyl/ π -alkyl	π -Sulfur
5a	-62.790	Phe-77, His-151	Phe-77, Phe-215	His-151, His-263	His-151, Ala-178, Leu-264	His-263
5b	-69.360	Phe-77, His-151	Phe-77, Phe-215	His-151, His-263	His-151, Ala-178, Phe-215, His-263, Leu-264	His-263
5c	-70.770	Phe-77, His-151	Phe-77, Phe-215	His-151, His-263	Phe-77, His-151, Ala-178, Leu-264	His-263
5d	-90.278	Phe-77, His-151	Phe-77, Tyr-114	His-151, His-263	His-151, Leu-153, Ala-178, Leu-264	His-263
5e	-95.740	Phe-77, His-151	Phe-77, Tyr-114	His-151, His-263	Tyr-114, His-151, Leu-153, Ala-178, Leu-264	His-263
5f	-89.950	Phe-77, His-151	Phe-77, Tyr-114	His-151, His-263	Tyr-114, His-151, Leu-153, Ala-178, Leu-264	His-263
5g	-81.790	Phe-77, His-151	Phe-77, Tyr-114	His-151, His-263	Gly-76, His-151, Leu-153, Ala-178, Leu-264	His-263
5h	-68.650	Gly-76, Phe-77, His-151	Phe-77, Phe-215	His-151, His-263	Ala-178, Leu-264	His-263
5i	-76.050	Gly-76, Phe-77, His-151	Phe-77, Phe-215	His-151, His-263	Ala-178, Phe-215, Leu-264	His-263
5j	-78.890	Gly-76, Phe-77, His-151	Phe-77, Phe-215	His-151, His-263	Phe-77, Ala-178, Leu-264	His-263
5k	-92.070	Gly-76, Phe-77	Phe-77, Tyr-114	His-151, His-263	Leu-153, Ala-178, Leu-264	His-263
5l	-80.390	Gly-76, Phe-77	Phe-77, Tyr-114	His-151, His-263	Tyr-114, Leu-153, Ala-178, Pro-180, Leu-264	His-263
5m	-74.530	Gly-76, Phe-77	Phe-77, Tyr-114	His-151, His-263	Tyr-114, Leu-153, Ala-178, Pro-180, Leu-264	His-263
5n	-72.330	Phe-77, His-151	---	His-263	Arg-256, Ala-260	His-263
5o	-66.840	Phe-77	Phe-77, Phe-215	Ser-152, His-263	Phe-77, Ala-178, Phe-215, Arg-256, Ala-259	His-263
5p	-73.820	Phe-77	Phe-77, Phe-215	Ser-152, His-263	Phe-77, Ala-178, Arg-256, Ala-259	His-263
5q	-72.620	Phe-77	Phe-77, Tyr-114	Ser-152, His-263	Leu-153, Ala-178, Pro-180, Arg-256, Ala-259	His-263
5r	-99.740	Phe-77	Phe-77, Tyr-114	His-263	Leu-153, Ala-178, Arg-256, Ala-259, Ala-260	Ser-152, His-263

Chapter V

...Contd

#	Mol Dock Score	H-bond	π - π interaction	π -cation	Alkyl/ π -alkyl	π -Sulfur
5s	-95.430	Phe-77	Phe-77, Phe-215	His-263	Phe-77, Ala-178, Arg-256, Ala-259	Ser-152, His-263
5t	-94.850	Phe-77	Phe-77, Phe-215	His-263	Leu-153, Ala-178, Arg-256, Ala-259, Ala-260	Ser-152, His-263
5u	-85.850	Phe-77	Phe-77, Phe-215	His-263	Phe-77, Ala-178, Arg-256, Ala-259	His-263
5v	-68.591	Gly-76, Phe-77, His-151	Phe-77, Tyr-114	His-151, His-263	Leu-153, Ala-178, Leu-264	His-263
5w	-80.410	Gly-76, Phe-77, His-151	--	His-263	Ala-259, Ala-260	His-263
5x	-75.720	Phe-77	Phe-77, Phe-215	His-263	Ala-178, Phe-215, Arg-256, Ala-259, Ala-260, Leu-264	Ser-152, His-263
5y	-94.260	Phe-77	Phe-77, Phe-215	His-263	Phe-77, Ala-178, Ala-259, Ala-260, Leu-264	Ser-152, His-263
5z	-67.700	Phe-77	Phe-77	His-263	Leu-153, Ala-178, Arg-256, Ala-259, Ala-260	Ser-152, His-263
5aa	-62.700	Phe-77	Phe-77	His-263	Leu-153, Ala-178, Arg-256, Ala-259, Ala-260	Ser-152, His-263
5ab	-68.020	Arg-256	Phe-77, Tyr-114	His-151, Arg-256, His-263,	Tyr-114, Pro-180, Ala-260, Leu-264	--
5ac	-74.950	Gly-76, Phe-77, His-151		Arg-256, His-263	Ala-259, Ala-260	His-263
5ad	-70.510	Phe-77	Phe-77, Phe-215	His-263	Ala-178, Phe-215, Ala-259, Ala-260, Leu-264	Ser-152, His-263
5ae	-93.470	Phe-77	Phe-77, Phe-215	His-263	Phe-77, Ala-178, Ala-259, Ala-260, Leu-264	Ser-152, His-263
5af	-72.391	Gly-76, Phe-77	Phe-77	Arg-256, His-263	Leu-153, Ala-178, Ala-259, Ala-260	His-263
5ag	-62.391	Phe-77	Phe-77, Tyr-114	His-263	Tyr-114, Leu-153, Ala-178, Pro-180, Arg-256, Ala-259, Ala-260	Ser-152, His-263
Orlistat	-107.750	Phe-77, Ser 152, His 263	Tyr-114, Trp-252	--	Arg-256, Ala-259,	--

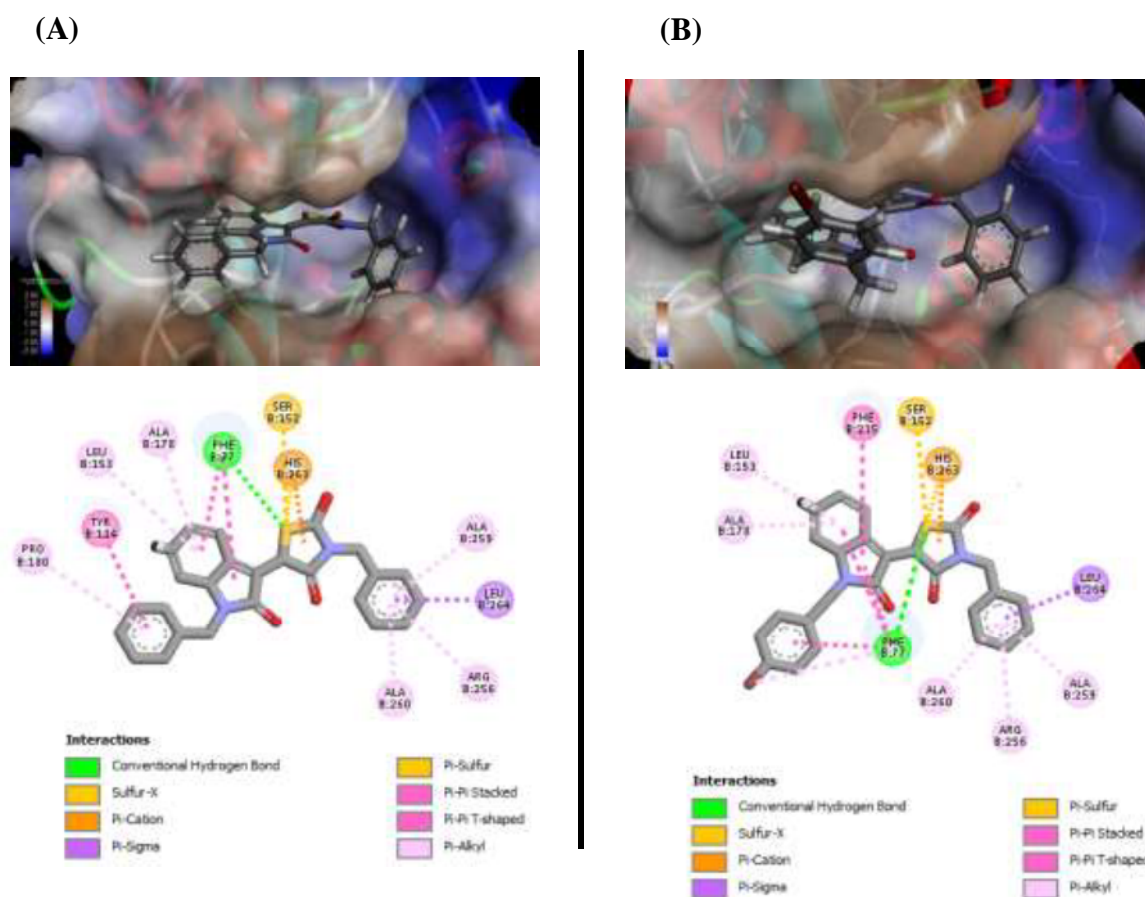


Fig. 5.7. Binding pose and 2D interaction diagram of **5r** (A) and **5t** (B) in the active site of PL (1LPB)

It is noteworthy that the benzyl substituted analogues (having potential PL inhibition) exerted an additional alkyl/ π -alkyl interaction over the alkyl counterpart. Previous literature suggests the potential role of Arg 256 in the opening of the hydrophobic lid domain [30-32]. Thus, the drastic potentiation in the PL inhibitory activity between the alkyl and aryl substituted analogues might be due to its interaction ability with the hydrophobic lid domain (open conformation) *via* alkyl/ π -alkyl interaction with the Arg 256. In case of orlistat, two types of interactions were primarily involved. A hydrogen bond interaction with Phe 77, Ser 152 and hydrophobic interaction with Tyr 114, Phe 215 and Arg 256 etc were formed during the docking simulations. The above results from the molecular docking study further supported the hypothesis, wherein both the aromatic substitutions on indole and TZD were helpful for the lid domain interactions, while the imide linkage in TZD interacted with the Ser 152.

Molecular modelling study suggested the probable role of the analogues for imparting various interactions with active site amino acids of 1LPB. Further, the stability of the

binding mode and interactions in a dynamic environment was evaluated by an optimised MD simulation. [14,17] In the MD run (GROMACS [33]), RMSD value reflected the stability of the complex structure, while RMSF value revealed the flexibility of a certain region of the macromolecule. Both the analogues (**5r** and **5t**) exhibited a stable binding conformation throughout the simulation with a maximum deviation of ≈ 0.8 nm at ≈ 10 ns (**Fig. 5.8**).

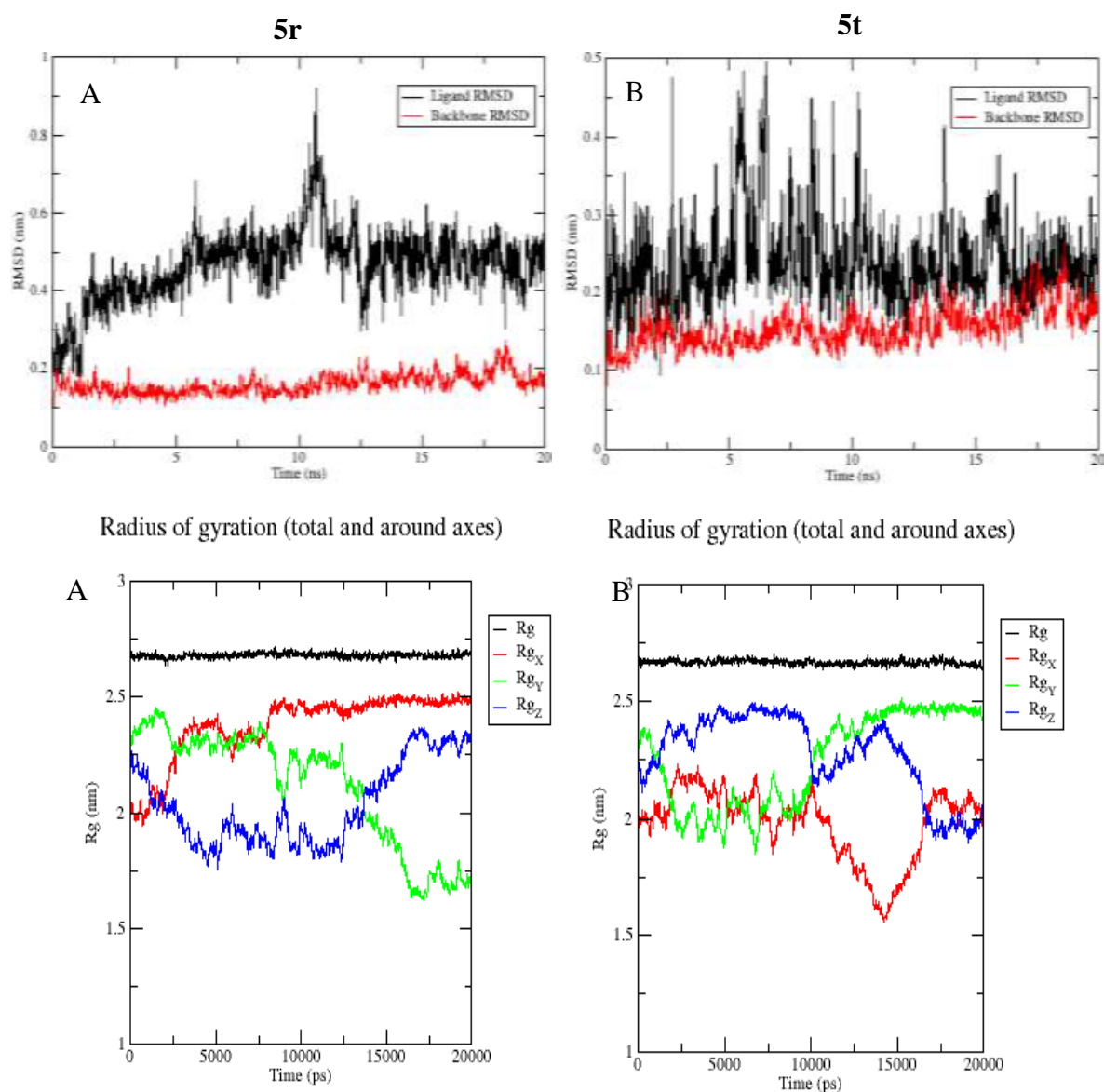


Fig. 5.8. RMSD of Ligands and Radius of gyrations retrieved from 20 ns MD simulations of the PL-ligand complex (A)- **5r**; (B)-**5t**.

The interactions of these analogues with 1LPB through the 20 ns are summarised in **Table 5.5**.

Chapter V

Table 5.5. Various interactions exhibited by **5r** and **5t** during the 20 ns MD run

Time (ns)	H Bond	π - π stacking	π -alkyl
5r			
0	Phe77, Asp 79	Phe 77, Phe 215	Ile 78, Arg 256, Ala 259
2	--	Phe 215	Ile 78, Ile 209, Arg 256, Ala 259, Ala 260, Leu 264
4	Arg 256	--	Ile 78, Ala 259, Ala 260
6	--	Phe 215, Phe 258	Ile 78, Arg 256, Ala 259, Ala 260
8	Arg 256	Phe 215, His 263	Ile 78, Leu 213, Ala 259, Ala 260, Leu 264
10	--	Phe 215	Ile 78, Ala 259, Ala 260, Leu 264
12	Arg 256	--	Ile 78, Ala 259, Ala 260, Leu 264
14	Arg 256	Phe 77	Ile 78, Ala 259, His 263, Leu 264
16	Arg 256	Phe 77, Phe 215	Ile 78, Ala 259, Ala 260, Leu 264
18	--	Phe 215	Ile 78, Arg 256, Ala 259, Ala 260, Leu 264
20	--	Phe 215, Phe 258	Ile 78, Arg 256, Ala 259, Ala 260, Leu 264
5t			
0	Phe77	Phe 77, Tyr 114, Phe 215	Ala 178, Ala 259
2	Ile 78	Phe 77, Phe 215	Arg 256, Ala 259
4	Ile 78, Arg 256	Phe 77, Phe 215	Arg 256, Ala 259, Ala 260
6	Ile 78	Phe 215, Trp 252	Ile 209, Leu 213, Arg 256, Ala 259, Ala 260
8	Ile 78	Phe 77, Phe 215, Trp 252, Thr 255	Leu 213, Arg 256, Ala 260
10	Ile 78	Phe 77, Phe 215	Arg 256, Ala 259, Ala 260
12	Ile 78, Arg 256	Phe 77	Ala 260
14	Arg 256	Phe 77, Phe 215, Thr 255	Arg 256, Ala 259, Ala 260
16	Arg 256	Phe 77, Trp 252	Ile 78, Ala 259, Ala 260
18	Arg 256	Phe 77, Phe 215, Trp 252	Arg 256, Ala 260
20	Arg 256	Phe 77, Phe 215, Trp 252	Ala 259, Ala 260

The analogues exhibited numerous interactions such as H bonding, π - π stacking and π -alkyl interactions etc. Initially, H bond interactions were formed with the lid domain amino acids (Phe 77, Ile 78 and Asp 79), later it turned to a stable interaction with Arg 256. π - π stacking interactions were observed with the aromatic amino acids (Phe 77, Phe 215), while π -alkyl interactions were observed with Ile 78, Arg 256, Ala 259, Ala 260, Leu 264 etc. Furthermore, a stable radius of gyration indicated the compactness of the 1LPB during the MD run with test analogues.

Chapter V

To summarize, a series of indole-TZD hybrid analogues (**5a** to **5ag**) were synthesized, characterized and evaluated for their *in-vitro* PL inhibition activity. Among the synthesized analogues, **5r** was found to be the most active inhibitor of PL with an IC_{50} of 7.30 μ M, followed by **5t** ($IC_{50} = 9.51 \mu$ M). Enzyme kinetics of these active analogues exhibited a competitive mode of enzyme inhibition. Fluorescence quenching studies further supported these facts wherein one binding site was evidently present in PL. Furthermore, molecular modelling studies validated the rationale for the selection of the hybrid analogues. A 20 ns MD simulation of the most active analogues (**5r** and **5t**)-PL highlighted a stable conformation in the dynamic environment.

Though, synthesized analogues exhibited a potential PL inhibition, it was envisaged that the inhibitory property can be further improved by the structural modifications. This is discussed in the next chapter.

References

- [1] R. Birari, S.K. Roy, A. Singh, K.K. Bhutani, Pancreatic lipase inhibitory alkaloids of *Murraya koenigii* leaves, *Nat. Prod. Commun.* 4 (2009) 1089–1092.
- [2] A.T.M.A. Rahim, Y. Takahashi, K. Yamaki, Mode of pancreatic lipase inhibition activity *in-vitro* by some flavonoids and non-flavonoid polyphenols, *Food Res. Int.* 75 (2015) 289–294.
- [3] S.N.C. Sridhar, S. Mutya, A.T. Paul, Bis-indole alkaloids from *Tabernaemontana divaricata* as potent pancreatic lipase inhibitors: Molecular modelling studies and experimental validation, *Med. Chem. Res.* 26 (2017) 1268–1278.
- [4] S.N.C. Sridhar, G. Ginson, P.O.V. Reddy, M.P. Tantak, D. Kumar, A.T. Paul, Synthesis, evaluation and molecular modelling studies of 2-(carbazol-3-yl)-2-oxoacetamide analogues as a new class of potential pancreatic lipase inhibitors, *Bioorg. Med. Chem.* 25 (2017) 609–620.
- [5] S.N.C. Sridhar, S. Palawat, A.T. Paul, Design, synthesis, biological evaluation and molecular modelling studies of indole glyoxylamides as a new class of potential pancreatic lipase inhibitors, *Bioorg. Chem.* 85 (2019) 373–381.
- [6] W. Han, Z. Hu, X. Jiang, C.P. Decicco, α -Ketoamides, α -Ketoesters and α -Diketones as HCV NS3 Protease Inhibitors, *Bioorg. Med. Chem. Lett.* 10 (2000) 711–713.
- [7] C. Steuer, C. Gege, W. Fischl, K.H. Heinonen, R. Bartenschlager, C.D. Klein, Synthesis and biological evaluation of α -ketoamides as inhibitors of the Dengue virus protease with antiviral activity in cell-culture, *Bioorg. Med. Chem.* 19 (2011) 4067–4074.
- [8] V. Point, A. Bénarouche, J. Zarrillo, A. Guy, R. Magnez, L. Fonseca, B. Raux, J. Leclaire, G. Buono, F. Fotiadu, others, Slowing down fat digestion and absorption by an oxadiazolone inhibitor targeting selectively gastric lipolysis, *Eur. J. Med. Chem.* 123 (2016) 834–848.
- [9] O. Bozdağ-Dündar, Ö. Özgen, A. Menteşe, N. Altanlar, O. Atli, E. Kendi, R. Ertan, Synthesis and antimicrobial activity of some new thiazolyl thiazolidine-2,4-dione derivatives, *Bioorg. Med. Chem.* 15 (2007) 6012–6017.

- [10] B.R. Bhattarai, B. Kafle, J.S. Hwang, S.W. Ham, K.H. Lee, H. Park, I.O. Han, H. Cho, Novel thiazolidinedione derivatives with anti-obesity effects: Dual action as PTP1B inhibitors and PPAR- γ activators, *Bioorg. Med. Chem. Lett.* 20 (2010) 6758–6763.
- [11] B.R. Bhattarai, B. Kafle, J.S. Hwang, D. Khadka, S.M. Lee, J.S. Kang, S.W. Ham, I.O. Han, H. Park, H. Cho, Thiazolidinedione derivatives as PTP1B inhibitors with antihyperglycemic and antiobesity effects, *Bioorg. Med. Chem. Lett.* 19 (2009) 6161–6165.
- [12] S.N.C. Sridhar, D. Bhurta, D. Kantiwal, G. George, V. Monga, A.T. Paul, Design, synthesis, biological evaluation and molecular modelling studies of novel diaryl substituted pyrazolyl thiazolidinediones as potent pancreatic lipase inhibitors, *Bioorg. Med. Chem. Lett.* 27 (2017) 3749–3754.
- [13] F.H.A. Leite, P.B.G. da S. Santiago, T.Q. Froes, J. da Silva Filho, S.G. da Silva, R.M. Ximenes, A.R. de Faria, D.J. Brondani, J.F.C. de Albuquerque, M.S. Castilho, Structure-guided discovery of thiazolidine-2,4-dione derivatives as a novel class of *Leishmania major* pteridine reductase 1 inhibitors, *Eur. J. Med. Chem.* 123 (2016) 639–648.
- [14] M.F. Abo-Ashour, W.M. Eldehna, R.F. George, M.M. Abdel-Aziz, M.M. Elaasser, N.M. Abdel Gawad, A. Gupta, S. Bhakta, S.M. Abou-Seri, Novel indole-thiazolidinone conjugates: Design, synthesis and whole-cell phenotypic evaluation as a novel class of antimicrobial agents, *Eur. J. Med. Chem.* 160 (2018) 49–60.
- [15] D.M. Corigliano, R. Syed, S. Messineo, A. Lupia, R. Patel, C.V.R. Reddy, P.K. Dubey, C. Colica, R. Amato, G. De Sarro, S. Alcaro, A. Indrasena, A. Brunetti, Indole and 2,4-Thiazolidinedione conjugates as potential anticancer modulators, *PeerJ.* 6 (2018) e5386.
- [16] K. Khaldoun, A. Safer, N. Boukabcha, N. Dege, S. Ruchaud, M. Souab, S. Bach, A. Chouaih, S. Saidi-Besbes, Synthesis and evaluation of new isatin-aminorhodanine hybrids as PIM1 and CLK1 kinase inhibitors, *J. Mol. Struct.* 1192 (2019) 82–90.
- [17] S.N.C. Sridhar, S. Palawat, A.T. Paul, Design, synthesis, biological evaluation and molecular modelling studies of conophylline inspired novel indolyl oxoacetamides as potent pancreatic lipase inhibitors, *New J. Chem.* 44 (2020) 12355–12369.

Chapter V

- [18] N.M. Evdokimov, I. V. Magedov, D. McBrayer, A. Kornienko, Isatin derivatives with activity against apoptosis-resistant cancer cells, *Bioorg. Med. Chem. Lett.* 26 (2016) 1558–1560.
- [19] L. Sun, N. Tran, F. Tang, H. App, P. Hirth, G. McMahon, C. Tang, Synthesis and biological evaluations of 3-substituted indolin-2-ones: A novel class of tyrosine kinase inhibitors that exhibit selectivity toward particular receptor tyrosine kinases, *J. Med. Chem.* 41 (1998) 2588–2603.
- [20] W. Fan, K.Y. Chen, Q.P. Chen, G. Li, B. Jiang, , *Org. Biomol. Chem.* 15 (2017) 6493–6499.
- [21] G. George, P.S. Dileep, A.T. Paul, Development and validation of a new HPTLC-HRMS method for the quantification of a potent pancreatic lipase inhibitory lead Echitamine from *Alstonia scholaris*, *Nat. Prod. Res.* (2019) 1–5.
- [22] H. Lineweaver, D. Burk, The determination of enzyme dissociation constants, *J. Am. Chem. Soc.* 56 (1934) 658–666.
- [23] B.T. Burlingham, T.S. Widlanski, An intuitive look at the relationship of K_i and IC_{50} : A more general use for the Dixon plot, *J. Chem. Educ.* 80 (2003) 214-217.
- [24] S. Li, J. Pan, X. Hu, Y. Zhang, D. Gong, G. Zhang, Kaempferol inhibits the activity of pancreatic lipase and its synergistic effect with orlistat, *J. Funct. Foods.* 72 (2020) 104041.
- [25] D.S. Reddy, M. Kongot, V. Singh, N. Maurya, R. Patel, N. Kumar Singhal, F. Avecilla, A. Kumar, Coumarin tethered cyclic imides as efficacious glucose uptake agents and investigation of hit candidate to probe its binding mechanism with human serum albumin, *Bioorg. Chem.* 92 (2019) 103212.
- [26] J.R. Lakowicz, Quenching of Fluorescence, in: J.R. Lakowicz (Ed.), *Princ. Fluoresc. Spectrosc.*, Springer science & business media, Boston, MA, 2006: pp. 277–330.
- [27] A.S. Ladokhin, Fluorescence Spectroscopy in Peptide and Protein Analysis, in: *Encycl. Anal. Chem.*, John Wiley & Sons, Ltd, Chichester, UK, 2000: pp. 529–536.
- [28] Y.T. Zhu, Y.W. Jia, Y.M. Liu, J. Liang, L.S. Ding, X. Liao, Lipase ligands in *Nelumbo nucifera* leaves and study of their binding mechanism, *J. Agric. Food*

Chem. 62 (2014) 10679–10686.

- [29] R. Thomsen, M.H. Christensen, MolDock: A new technique for high-accuracy molecular docking, *J. Med. Chem.* 49 (2006) 3315–3321.
- [30] M.E. Lowe, Pancreatic triglyceride lipase and colipase: Insights into dietary fat digestion, *Gastroenterology*. 107 (1994) 1524–1536.
- [31] M.E. Lowe, Structure and Function of Pancreatic Lipase and Colipase, *Annu. Rev. Nutr.* 17 (2002) 141–158.
- [32] R.B. Birari, S. Gupta, C.G. Mohan, K.K. Bhutani, Antiobesity and lipid lowering effects of *Glycyrrhiza* chalcones: Experimental and computational studies, *Phytomedicine*. 18 (2011) 795–801.
- [33] M.J. Abraham, T. Murtola, R. Schulz, S. Páll, J.C. Smith, B. Hess, E. Lindahl, GROMACS: High performance molecular simulations through multi-level parallelism from laptops to supercomputers, *SoftwareX*. 1 (2015) 19–25.